

# GUARD: A Safe Reinforcement Learning Benchmark

**Weiye Zhao**

Robotics Institute

Carnegie Mellon University

weiyezha@andrew.cmu.edu

**Rui Chen**

Robotics Institute

Carnegie Mellon University

ruic3@andrew.cmu.edu

**Yifan Sun**

Robotics Institute

Carnegie Mellon University

yifansu2@andrew.cmu.edu

**Ruixuan Liu**

Robotics Institute

Carnegie Mellon University

ruixuanl@andrew.cmu.edu

**Tianhao Wei**

Robotics Institute

Carnegie Mellon University

twei2@andrew.cmu.edu

**Changliu Liu**

Robotics Institute

Carnegie Mellon University

cliu6@andrew.cmu.edu

## Abstract

Due to the trial-and-error nature, it is typically challenging to apply RL algorithms to safety-critical real-world applications, such as autonomous driving, human-robot interaction, robot manipulation, etc, where such errors are not tolerable. Recently, safe RL (*i.e.*, constrained RL) has emerged rapidly in the literature, in which the agents explore the environment while satisfying constraints. Due to the diversity of algorithms and tasks, it remains difficult to compare existing safe RL algorithms. To fill that gap, we introduce GUARD, a Generalized Unified SAFe Reinforcement Learning Development Benchmark. GUARD has several advantages compared to existing benchmarks. First, GUARD is a generalized benchmark with a wide variety of RL agents, tasks, and safety constraint specifications. Second, GUARD comprehensively covers state-of-the-art safe RL algorithms with self-contained implementations. Third, GUARD is highly customizable in tasks and algorithms. We present a comparison of state-of-the-art safe RL algorithms in various task settings using GUARD and establish baselines that future work can build on.

## 1 Introduction

Reinforcement learning (RL) has achieved tremendous success in many fields over the past decades. In RL tasks, the agent explores and interacts with the environment by trial and error, and improves its performance by maximizing the long-term reward signal. RL algorithms enable the development of intelligent agents that can achieve human-competitive performance in a wide variety of tasks, such as games [Mnih et al., 2013, Zhao et al., 2019a, Silver et al., 2018, OpenAI et al., 2019, Vinyals et al., 2019, Zhao et al., 2019b], manipulation [Popov et al., 2017, Zhao et al., 2022a, Chen et al., 2023, Agostinelli et al., 2019, Shek et al., 2022, Zhao et al., 2020a, Noren et al., 2021], autonomous driving [Isele et al., 2019, Kiran et al., 2022, Gu et al., 2022a], robotics [Kober et al., 2013, Brunke et al., 2022, Zhao et al., 2022b, 2020b, Sun et al., 2023, Cheng et al., 2019], and more. Despite their outstanding performance in maximizing rewards, recent works [Garcia and Fernández, 2015, Gu et al., 2022b, Zhao et al., 2023] focus on the safety aspect of training and deploying RL algorithms due to the safety concern [Zhao et al., 2022c, He et al., 2023a, Wei et al., 2022] in real-world safety-critical applications, *e.g.*, human-robot interaction, autonomous driving, etc. As safe RL topics emerge in the literature [Zhao et al., 2021, 2023, He et al., 2023b], it is crucial to employ a standardized benchmark for comparing and evaluating the performance of various safe RL algorithms across different applications, ensuring a reliable transition from theory to practice. A benchmark includes 1) algorithms for comparison; 2) environments to evaluate algorithms; 3) a set of evaluation metrics, etc. There are benchmarks for unconfined RL and some safe RL, but not comprehensive enough [Duan

et al., 2016, Brockman et al., 2016, Ellenberger, 2018–2019, Yu et al., 2019, Osband et al., 2020, Tunyasuvunakool et al., 2020, Dulac-Arnold et al., 2020, Zhang et al., 2022a].

To create a robust safe RL benchmark, we identify three essential pillars. Firstly, the benchmark must be **generalized**, accommodating diverse agents, tasks, and safety constraints. Real-world applications involve various agent types (e.g., drones, robot arms) with distinct complexities, such as different control degrees-of-freedom (DOF) and interaction modes (e.g., 2D planar or 3D spatial motion). The performance of algorithms is influenced by several factors, including variations in robots (such as observation and action space dimensions), tasks (interactive or non-interactive, 2D or 3D), and safety constraints (number, trespassibility, movability, and motion space). Therefore, providing a comprehensive environment to test the generalizability of safe RL algorithms is crucial.

Secondly, the benchmark should be **unified**, overcoming discrepancies in experiment setups prevalent in the emerging safe RL literature. A unified platform ensures consistent evaluation of different algorithms in controlled environments, promoting reliable performance comparison. Lastly, the benchmark must be **extensible**, allowing researchers to integrate new algorithms and extend setups to address evolving challenges. Given the ongoing progress in safe RL, the benchmark should incorporate major existing works and adapt to advancements. By encompassing these pillars, the benchmark provides a solid foundation for addressing these open problems in safe RL research.

In light of the above-mentioned pillars, this paper introduces GUARD, a Generalized Unified SAFe Reinforcement Learning Development Benchmark. The code is available on Github<sup>1</sup>. In particular, GUARD is developed based upon the Safety Gym [Ray et al., 2019], SafeRL-Kit [Zhang et al., 2022a] and SpinningUp [Achiam, 2018]. Unlike existing benchmarks, GUARD pushes the boundary beyond the limit by significantly extending the algorithms in comparison , types of agents and tasks, and safety constraint specifications. The contributions of this paper are as follows:

1. **Generalized benchmark with a wide range of agents.** GUARD genuinely supports **11** different agents, covering the majority of real robot types.
2. **Generalized benchmark with a wide range of tasks.** GUARD genuinely supports **7** different task specifications, which can be combined to represent most real robot tasks.
3. **Generalized benchmark with a wide range of safety constraints.** GUARD genuinely supports **8** different safety constraint specifications. The included constraint options comprehensively cover the safety requirements that would encounter in real-world applications.
4. **Unified benchmarking platform with comprehensive coverage of safe RL algorithms.** GUARD implements **8** state-of-the-art safe RL algorithms following a unified code structure.
5. **Highly customizable benchmarking platform.** GUARD features a modularized design that enables effortless customization of new testing suites with self-customizable agents, tasks, and constraints. The algorithms in GUARD are self-contained, with a consistent structure and independent implementations, ensuring clean code organization and eliminating dependencies between different algorithms. This self-contained structure greatly facilitates the seamless integration of new algorithms for further extensions.

## 2 Related Work

**Open-source Libraries for Reinforcement Learning Algorithms** Open-source RL libraries are code bases that implement representative RL algorithms for efficient deployment and comparison. They often serve as backbones for developing new RL algorithms, greatly facilitating RL research. We divide existing libraries into two categories: (a) safety-oriented RL libraries that support safe RL algorithms, and (b) general RL libraries that do not. Among safety-oriented libraries, Safety Gym [Ray et al., 2019] is the most famous one with highly configurable tasks and constraints but only supports three safe RL methods. SafeRL-Kit [Zhang et al., 2022a] supports five safe RL methods while missing some key methods such as CPO [Achiam et al., 2017a]. Bullet-Safety-Gym [Gronauer, 2022] supports CPO but is limited in overall safe RL support at totally four methods. Compared to the above libraries, our proposed GUARD doubles the support at eight methods in total, covering a wider spectrum of general safe RL research. General RL libraries, on the other hand, can be summarized according to their backend into PyTorch [Achiam, 2018, Weng et al., 2022, Raffin et al., 2021, Liang

---

<sup>1</sup><https://github.com/intelligent-control-lab/guard>

et al., 2018], Tensorflow [Dhariwal et al., 2017, Hill et al., 2018], Jax [Castro et al., 2018, Hoffman et al., 2020], and Keras [Plappert, 2016]. In particular, SpinningUp [Achiam, 2018] serves as the major backbone of our GUARD benchmark on the safety-agnostic RL portion.

**Benchmark Platform for Safe RL Algorithms** To facilitate safe RL research, the benchmark platform should support a wide range of task objectives, constraints, and agent types. Among existing work, the most representative one is Safety Gym [Ray et al., 2019] which is highly configurable. However, Safety Gym is limited in agent types in that it does not support high-dimensional agents (e.g., drone and arm) and lacks tasks with complex interactions (e.g., chase and defense). Moreover, Safety Gym only supports naive contact dynamics (e.g., touch and snap) instead of more realistic cases (e.g., objects bouncing off upon contact) in contact-rich tasks. Safe Control Gym [Yuan et al., 2022] is another open-source platform that supports very simple dynamics (i.e., cartpole, 1D/2D quadrotors) and only supports navigation tasks. Finally, Bullet Safety Gym [Gronauer, 2022] provides high-fidelity agents, but the types of agents are limited, and they only consider navigation tasks. Compared to the above platforms, our GUARD supports a much wider range of task objectives (e.g., 3D reaching, chase and defense) with a much larger variety of eight agents including high-dimensional ones such as drones, arms, ants, and walkers.

### 3 Preliminaries

**Markov Decision Process** An Markov Decision Process (MDP) is specified by a tuple  $(\mathcal{S}, \mathcal{A}, \gamma, \mathcal{R}, P, \rho)$ , where  $\mathcal{S}$  is the state space, and  $\mathcal{A}$  is the control space,  $\mathcal{R} : \mathcal{S} \times \mathcal{A} \rightarrow \mathbb{R}$  is the reward function,  $0 \leq \gamma < 1$  is the discount factor,  $\rho : \mathcal{S} \rightarrow [0, 1]$  is the starting state distribution, and  $P : \mathcal{S} \times \mathcal{A} \times \mathcal{S} \rightarrow [0, 1]$  is the transition probability function (where  $P(s'|s, a)$  is the probability of transitioning to state  $s'$  given that the previous state was  $s$  and the agent took action  $a$  at state  $s$ ). A stationary policy  $\pi : \mathcal{S} \rightarrow \mathcal{P}(\mathcal{A})$  is a map from states to a probability distribution over actions, with  $\pi(a|s)$  denoting the probability of selecting action  $a$  in state  $s$ . We denote the set of all stationary policies by  $\Pi$ . Suppose the policy is parameterized by  $\theta$ ; policy search algorithms search for the optimal policy within a set  $\Pi_\theta \subset \Pi$  of parameterized policies.

The solution of the MDP is a policy  $\pi$  that maximizes the performance measure  $\mathcal{J}(\pi)$  computed via the discounted sum of reward:

$$\mathcal{J}(\pi) = \mathbb{E}_{\tau \sim \pi} \left[ \sum_{t=0}^{\infty} \gamma^t \mathcal{R}(s_t, a_t, s_{t+1}) \right], \quad (1)$$

where  $\tau = [s_0, a_0, s_1, \dots]$  is the state and control trajectory, and  $\tau \sim \pi$  is shorthand for that the distribution over trajectories depends on  $\pi : s_0 \sim \mu, a_t \sim \pi(\cdot|s_t), s_{t+1} \sim P(\cdot|s_t, a_t)$ . Let  $R(\tau) \doteq \sum_{t=0}^{\infty} \gamma^t \mathcal{R}(s_t, a_t, s_{t+1})$  be the discounted return of a trajectory. We define the on-policy value function as  $V^\pi(s) \doteq \mathbb{E}_{\tau \sim \pi}[R(\tau)|s_0 = s]$ , the on-policy action-value function as  $Q^\pi(s, a) \doteq \mathbb{E}_{\tau \sim \pi}[R(\tau)|s_0 = s, a_0 = a]$ , and the advantage function as  $A^\pi(s, a) \doteq Q^\pi(s, a) - V^\pi(s)$ .

**Constrained Markov Decision Process** A constrained Markov Decision Process (CMDP) is an MDP augmented with constraints that restrict the set of allowable policies. Specifically, CMDP introduces a set of cost functions,  $C_1, C_2, \dots, C_m$ , where  $C_i : \mathcal{S} \times \mathcal{A} \times \mathcal{S} \rightarrow \mathbb{R}$  maps the state action transition tuple into a cost value. Similar to (1), we denote  $\mathcal{J}_{C_i}(\pi) = \mathbb{E}_{\tau \sim \pi}[\sum_{t=0}^{\infty} \gamma^t C_i(s_t, a_t, s_{t+1})]$  as the cost measure for policy  $\pi$  with respect to the cost function  $C_i$ . Hence, the set of feasible stationary policies for CMDP is then defined as  $\Pi_C = \{\pi \in \Pi \mid \forall i, \mathcal{J}_{C_i}(\pi) \leq d_i\}$ , where  $d_i \in \mathbb{R}$ . In CMDP, the objective is to select a feasible stationary policy  $\pi$  that maximizes the performance:

$\max_{\pi \in \Pi_\theta \cap \Pi_C} \mathcal{J}(\pi)$ . Lastly, we define on-policy value, action-value, and advantage functions for the cost as  $V_{C_i}^\pi, Q_{C_i}^\pi$  and  $A_{C_i}^\pi$ , which are analogous to  $V^\pi, Q^\pi$ , and  $A^\pi$ , with  $C_i$  replacing  $R$ .

### 4 GUARD Safe RL Library

#### 4.1 Overall Implementation

GUARD contains the latest methods that can achieve safe RL: (i) end-to-end safe RL algorithms including CPO [Achiam et al., 2017a], TRPO-Lagrangian [Bohez et al., 2019], TRPO-FAC [Ma

et al., 2021], TRPO-IPO [Liu et al., 2020], and PCPO [Yang et al., 2020]; and (ii) hierarchical safe RL algorithms including TRPO-SL (TRPO-Safety Layer) [Dalal et al., 2018] and TRPO-USL (TRPO-Unrolling Safety Layer) [Zhang et al., 2022a]. We also include TRPO [Schulman et al., 2015] as an unconstrained RL baseline. Note that GUARD only considers model-free approaches which rely less on assumptions than model-based ones. We highlight the benefits of our algorithm implementations in GUARD:

- GUARD comprehensively covers a **wide range of algorithms** that enforce safety in both hierarchical and end-to-end structures. Hierarchical methods maintain a separate safety layer, while end-to-end methods solve the constrained learning problem as a whole.
- GUARD provides a **fair comparison among safety components** by equipping every algorithm with the same reward-oriented RL backbone (i.e., TRPO [Schulman et al., 2015]), implementation (i.e., MLP policies with [64, 64] hidden layers and tanh activation), and training procedures. Hence, all algorithms inherit the performance guarantee of TRPO.
- GUARD is implemented in PyTorch with a clean structure where every algorithm is self-contained, enabling **fast customization and development** of new safe RL algorithms. GUARD also comes with unified logging and plotting utilities which makes analysis easy.

## 4.2 Unconstrained RL

**TRPO** We include TRPO [Schulman et al., 2015] since it is state-of-the-art and several safe RL algorithms are based on it. TRPO is an unconstrained RL algorithm and only maximizes performance  $\mathcal{J}$ . The key idea behind TRPO is to iteratively update the policy within a local range (trust region) of the most recent version  $\pi_k$ . Mathematically, TRPO updates policy via

$$\pi_{k+1} = \underset{\pi \in \Pi_\theta}{\operatorname{argmax}} \mathcal{J}(\pi) \quad \text{s.t. } \mathcal{D}_{KL}(\pi, \pi_k) \leq \delta, \quad (2)$$

where  $\mathcal{D}_{KL}$  is Kullback-Leibler (KL) divergence,  $\delta > 0$  and the set  $\{\pi \in \Pi_\theta : \mathcal{D}_{KL}(\pi, \pi_k) \leq \delta\}$  is called the *trust region*. To solve (2), TRPO applies Taylor expansion to the objective and constraint at  $\pi_k$  to the first and second order, respectively. That results in an approximate optimization with linear objective and quadratic constraints (LOQC). TRPO guarantees a worst-case performance degradation.

## 4.3 End-to-End Safe RL

**CPO** Constrained Policy Optimizaiton (CPO) [Achiam et al., 2017b] handles CMDP by extending TRPO. Similar to TRPO, CPO also performs local policy updates in a trust region. Different from TRPO, CPO additionally requires  $\pi_{k+1}$  to be constrained by  $\Pi_\theta \cap \Pi_C$ . For practical implementation, CPO replaces the objective and constraints with surrogate functions (advantage functions), which can easily be estimated from samples collected on  $\pi_k$ , formally:

$$\begin{aligned} \pi_{k+1} = \underset{\pi \in \Pi_\theta}{\operatorname{argmax}} \quad & \mathbb{E}_{\substack{s \sim d^{\pi_k} \\ a \sim \pi}} [A^{\pi_k}(s, a)] \\ \text{s.t. } & \mathcal{D}_{KL}(\pi, \pi_k) \leq \delta, \quad \mathcal{J}_{C_i}(\pi_k) + \frac{1}{1 - \gamma} \mathbb{E}_{\substack{s \sim d^{\pi_k} \\ a \sim \pi}} \left[ A_{C_i}^{\pi_k}(s, a) \right] \leq d_i, i = 1, \dots, m. \end{aligned} \quad (3)$$

where  $d^{\pi_k} \doteq (1 - \gamma) \sum_{t=0}^H \gamma^t P(s_t = s | \pi_k)$  is the discounted state distribution. Following TRPO, CPO also performs Taylor expansion on the objective and constraints, resulting in a Linear Objective with Linear and Quadratic Constraints (LOLQC). CPO inherits the worst-case performance degradation guarantee from TRPO and has a worst-case cost violation guarantee.

**PCPO** Projection-based Constrained Policy Optimization (PCPO) [Yang et al., 2020] is proposed based on CPO, where PCPO first maximizes reward using a trust region optimization method without any constraints, then PCPO reconciles the constraint violation (if any) by projecting the policy back onto the constraint set. Policy update then follows an analytical solution:

$$\pi_{k+1} = \pi_k + \sqrt{\frac{2\delta}{g^\top H^{-1} g}} H^{-1} g - \max \left( 0, \frac{\sqrt{\frac{2\delta}{g^\top H^{-1} g}} g_c^\top H^{-1} g + b}{g_c^\top L^{-1} g_c} \right) L^{-1} g_c \quad (4)$$

where  $g_c$  is the gradient of the cost advantage function,  $g$  is the gradient of the reward advantage function,  $H$  is the Hessian of the KL divergence constraint,  $b$  is the constraint violation of the policy  $\pi_k$ ,  $L = \mathcal{I}$  for  $L_2$  norm projection, and  $L = H$  for KL divergence projection. PCPO provides a lower bound on reward improvement and an upper bound on constraint violation.

**TRPO-Lagrangian** Lagrangian methods solve constrained optimization by transforming hard constraints into soft constraints in the form of penalties for violations. Given the objective  $\mathcal{J}(\pi)$  and constraints  $\{\mathcal{J}_{C_i}(\pi) \leq d_i\}_i$ , TRPO-Lagrangian [Bohez et al., 2019] first constructs the dual problem

$$\max_{\forall i, \lambda_i \geq 0} \min_{\pi \in \Pi_\theta} -\mathcal{J}(\pi) + \sum_i \lambda_i (\mathcal{J}_{C_i}(\pi) - d_i). \quad (5)$$

The update of  $\theta$  is done via a trust region update with the objective of (2) replaced by that of (5) while fixing  $\lambda_i$ . The update of  $\lambda_i$  is done via standard gradient ascend. Note that TRPO-Lagrangian does not have a theoretical guarantee for constraint satisfaction.

**TRPO-FAC** Inspired by Lagrangian methods and aiming at enforcing state-wise constraints (e.g., preventing state from stepping into infeasible parts in the state space), Feasible Actor Critic (FAC) [Ma et al., 2021] introduces a multiplier (dual variable) network. Via an alternative update procedure similar to that for (5), TRPO-FAC solves the *statewise* Lagrangian objective:

$$\max_{\forall i, \xi_i} \min_{\pi \in \Pi_\theta} -\mathcal{J}(\pi) + \sum_i \mathbb{E}_{s \sim d^{\pi_k}} [\lambda_{\xi_i}(s)(\mathcal{J}_{C_i}(\pi) - d_i)], \quad (6)$$

where  $\lambda_{\xi_i}(s)$  is a parameterized Lagrangian multiplier network and is parameterized by  $\xi_i$  for the  $i$ -th constraint. Note that TRPO-FAC does not have a theoretical guarantee for constraint satisfaction.

**TRPO-IPO** TRPO-IPO [Liu et al., 2020] incorporates constraints by augmenting the optimization objective in (2) with logarithmic barrier functions, inspired by the interior-point method [Boyd and Vandenberghe, 2004]. Ideally, the augmented objective is  $I(\mathcal{J}_{C_i}(\pi) - d_i) = 0$  if  $\mathcal{J}_{C_i}(\pi) - d_i \leq 0$  or  $-\infty$  otherwise. Intuitively, that enforces the constraints since the violation penalty would be  $-\infty$ . To make the objective differentiable,  $I(\cdot)$  is approximated by  $\phi(x) = \log(-x)/t$  where  $t > 0$  is a hyperparameter. Then TRPO-IPO solves (2) with the objective replaced by  $\mathcal{J}_{\text{IPO}}(\pi) = \mathcal{J}(\pi) + \sum_i \phi(\mathcal{J}_{C_i}(x) - d_i)$ . TRPO-IPO does not have theoretical guarantees for constraint satisfaction.

#### 4.4 Hierarchical Safe RL

**Safety Layer** Safety Layer [Dalal et al., 2018], added on top of the original policy network, conducts a quadratic-programming-based constrained optimization to project reference action into the nearest safe action. Mathematically:

$$a_t^{safe} = \underset{a}{\operatorname{argmin}} \frac{1}{2} \|a - a_t^{ref}\|^2 \quad \text{s.t.} \quad \forall i, \bar{g}_{\varphi_i}(s_t)^\top a + C_i(s_{t-1}, a_{t-1}, s_t) \leq d_i \quad (7)$$

where  $a_t^{ref} \sim \pi_k(\cdot | s_t)$ , and  $\bar{g}_{\varphi_i}(s_t)^\top a_t + C_i(s_{t-1}, a_{t-1}, s_t) \approx C_i(s_t, a_t, s_{t+1})$  is a  $\varphi$  parameterized linear model. If there's only one constraint, (7) has a closed-form solution.

**USL** Unrolling Safety Layer (USL) [Zhang et al., 2022b] is proposed to project the reference action into safe action via gradient-based correction. Specifically, USL iteratively updates the learned  $Q_C(s, a)$  function with the samples collected during training. With step size  $\eta$  and normalization factor  $\mathcal{Z}$ , USL performs gradient descent as  $a_t^{safe} = a_t^{ref} - \frac{\eta}{\mathcal{Z}} \cdot \frac{\partial}{\partial a_t^{ref}} [Q_C(s_t, a_t^{ref}) - d]$ .

## 5 GUARD Testing Suite

### 5.1 Robot Options

In GUARD testing suite, the agent (in the form of a robot) perceives the world through sensors and interacts with the world through actuators. Robots are specified through MuJoCo XML files. The suite is equipped with 8 types of pre-made robots that we use in our benchmark environments as shown in Figure 1. The action space of the robots are continuous, and linearly scaled to  $[-1, +1]$ .

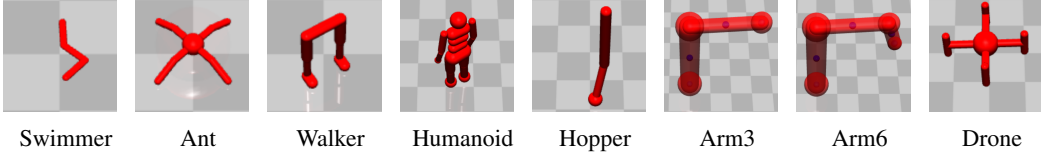


Figure 1: Robots of our environments.

**Swimmer** consist of three links and two joints. Each joint connects two links to form a linear chain. Swimmer can move around by applying **2** torques on the joints.

**Ant** is a quadrupedal robot composed a torso and four legs. Each of the four legs has a hip joint and a knee joint; and can move around by applying **8** torques to the joints.

**Walker** is a bipedal robot that consists of four main parts - a torso, two thighs, two legs, and two feet. Different from the knee joints and the ankle joints, each of the hip joints has three hinges in the  $x$ ,  $y$  and  $z$  coordinates to help turning. With the torso height fixed, Walker can move around by controlling **10** joint torques.

**Humanoid** is also a bipedal robot that has a torso with a pair of legs and arms. Each leg of Humanoid consists of two joints (no ankle joint). Since we mainly focus on the navigation ability of the robots in designed tasks, the arm joints of Humanoid are fixed, which enables Humanoid to move around by only controlling **6** torques.

**Hopper** is a one-legged robot that consists of four main parts - a torso, a thigh, a leg, and a single foot. Similar to Walker, Hopper can move around by controlling **5** joint torques.

**Arm3** is designed to simulate a fixed three-joint robot arm. Arm is equipped with multiple sensors on each links in order to fully observe the environment. By controlling **3** joint torques, Arm can move its end effector around with high flexibility.

**Arm6** is designed to simulate a robot manipulator with a fixed base and six joints. Similar to Arm3, Arm6 can move its end effector around by controlling **6** torques.

**Drone** is designed to simulate a quadrotor. The interaction between the quadrotor and the air is simulated by applying four external forces on each of the propellers. The external forces are set to balance the gravity when the control action is zero. Drone can move in 3D space by applying **4** additional control forces on the propellers.

## 5.2 Task Options

We categorize robot tasks in two ways: (i) interactive versus non-interactive tasks, and (ii) 2D space versus 3D space tasks. 2D space tasks constrain agents to a planar space, while 3D space tasks do not. Non-interactive tasks primarily involve achieving a target state (e.g., trajectory tracking) while interactive tasks (e.g., human-robot collaboration and unstructured object pickup) necessitate contact or non-contact interactions between the robot and humans or movable objects, rendering them more challenging. On a variety of tasks that cover different situations, GUARD facilitates a thorough evaluation of safe RL algorithms via the following tasks. See Table 17 for more information.

**Goal** (Figure 2a) requires the robot navigating towards a series of 2D or 3D goal positions. Upon reaching a goal, the location is randomly reset. The task provides a sparse reward upon goal achievement and a dense reward for making progress toward the goal.

**Push** (Figure 2b) requires the robot pushing a ball toward different goal positions. The task includes a sparse reward for the ball reaching the goal circle and a dense reward that encourages the agent to approach both the ball and the goal. Unlike pushing a box in Safety Gym, it is more challenging to push a ball since the ball can roll away and the contact dynamics are more complex.

**Chase** (Figure 2c) requires the robot tracking multiple dynamic targets. Those targets continuously move away from the robot at a slow speed. The dense reward component provides a bonus for minimizing the distance between the robot and the targets. The targets are constrained to a circular area. A 3D version of this task is also available, where the targets move within a restricted 3D space. Detailed dynamics of the targets is described in Appendix A.5.1.

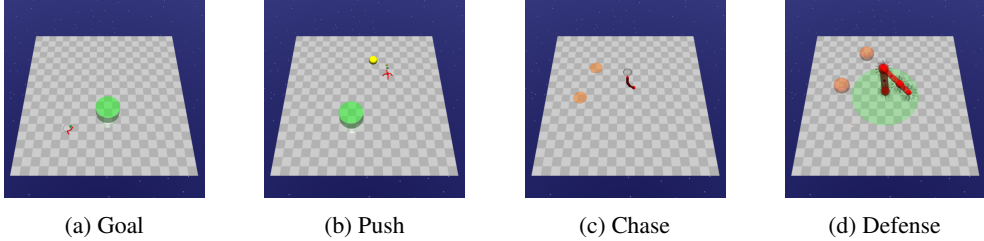


Figure 2: Tasks of our environments.

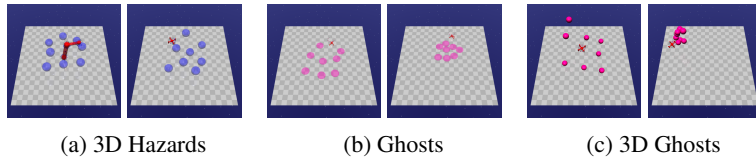


Figure 3: Constraints of our environments.

**Defense** (Figure 2d) requires the robot to prevent dynamic targets from entering a protected circle area. The targets will head straight toward the protected area or avoid the robot if the robot gets too close. Dense reward component provides a bonus for increasing the cumulative distance between the targets and the protected area. Detailed dynamics of the targets is described in Appendix A.5.2.

### 5.3 Constraint Options

We classify constraints based on various factors: **trespassability**: whether constraints are trespassable or untrespassable. Trespassable constraints allow violations without causing any changes to the robot’s behaviors, and vice versa. (ii) **movability**: whether they are immovable, passively movable, or actively movable; and (iii) **motion space**: whether they pertain to 2D or 3D environments. To cover a comprehensive range of constraint configurations, we introduce additional constraint types via expanding Safety Gym. Please refer to Table 18 for all configurable constraints.

**3D Hazards** (Figure 3a) are dangerous 3D areas to avoid. These are floating spheres that are trespassable, and the robot is penalized for entering them.

**Ghosts** (Figure 3b) are dangerous areas to avoid. Different from hazards, ghosts always move toward the robot slowly, represented by circles on the ground. Ghosts can be either trespassable or untrespassable. The robot is penalized for touching the untrespassable ghosts and entering the trespassable ghosts. Moreover, ghosts can be configured to start chasing the robot when the distance from the robot is larger than some threshold. This feature together with the adjustable velocity allows users to design the ghosts with different aggressiveness. Detailed dynamics of the targets is described in Appendix A.5.3.

**3D Ghosts** (Figure 3c) are dangerous 3D areas to avoid. These are floating spheres as 3D version of ghosts, sharing the similar behaviour with ghosts.

## 6 GUARD Experiments

**Benchmark Suite** GUARD includes a set of predefined benchmark testing suite in form of {Task}\_{Robot}\_{Constraint Number}{Constraint Type}. The full list of our testing suite can be found in Table 20.

**Benchmark Results** The summarized results can be found in Tables 21 to 25, and the learning rate curves are presented in Figures 6 to 10. As shown in Figure 4, we select 8 set of results to demonstrate the performance of different robot, task and constraints in GUARD. At a high level, the experiments show that all methods can consistently improve reward performance.

When comparing constrained RL methods to unconstrained RL methods, the former exhibit superior performance in terms of cost reduction. By incorporating constraints into the RL framework, the robot

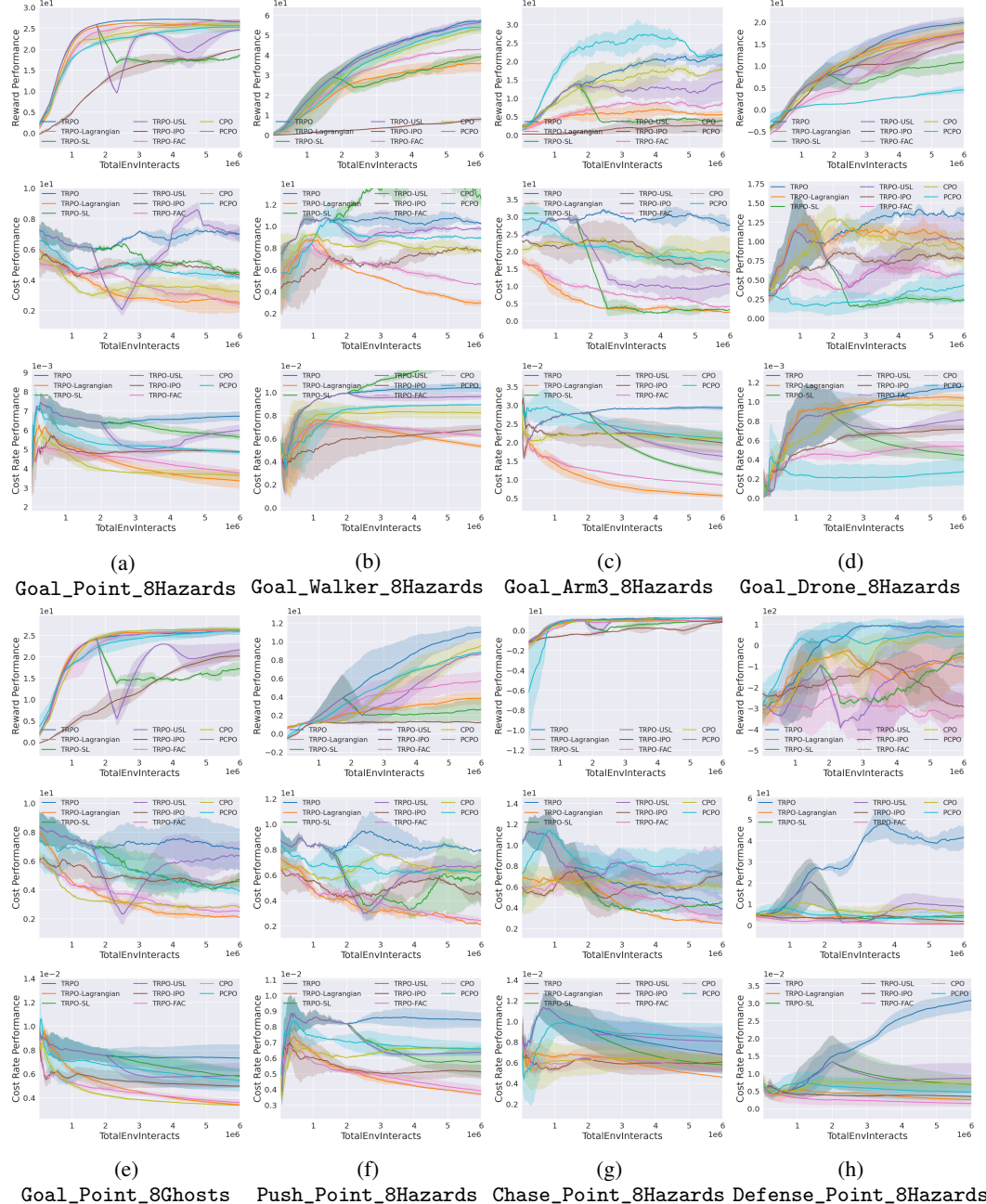


Figure 4: Comparison of results from four representative tasks. (a) to (d) cover four robots on the goal task. (e) shows the performance of a task with ghosts. (f) to (h) cover three different tasks with the point robot.

can navigate its environment while minimizing costs. This feature is particularly crucial for real-world applications where the avoidance of hazards and obstacles is of utmost importance. Nevertheless, it is important to point out that hierarchical RL methods (i.e., TRPO-SL and TRPO-USL) result in a trade-off between reward performance and cost reduction. While these methods excel at minimizing costs, they may sacrifice some degree of reward attainment in the process.

As shown in Figures 4b and 4c, tasks that involve high-dimensional robot action spaces and complex workspaces suffer from slower convergence due to the increased complexity of the learning problem. Moreover, the presence of dynamic ghosts in our tasks introduces further complexities. These tasks exhibit higher variance during the training process due to the collision-inducing behaviors of the dynamic ghosts. The robot must adapt and respond effectively to the ghosts' unpredictable movements. Addressing these challenges requires robust algorithms capable of handling the dynamic nature of the ghosts while optimizing the robot's overall performance. The influence of ghosts is evident by comparing Figure 4a and 4e, where the variance of cost performance increases with ghosts for several methods (e.g., PCPO and USL).

Figure 4a, 4f, 4g, and 4h illustrate the performance of a point robot on four distinct tasks. It is evident that the chase task exhibits the quickest convergence, while the defense task reveals the most performance gaps between methods. These verify that GUARD effectively benchmarks different methods under diverse scenarios.

## 7 Conclusions

Applying RL algorithms to safety-critical real-world applications poses significant challenges due to their trial-and-error nature. To address the problem, the literature has witnessed a rapid emergence of safe RL (constrained RL) approaches, where agents explore the environment while adhering to safety constraints. However, comparing diverse safe RL algorithms remains challenging. This paper introduces GUARD, the Generalized Unified SAfe Reinforcement Learning Development Benchmark. GUARD offers several advantages over existing benchmarks. Firstly, it provides a generalized framework with a wide range of RL agents, tasks, and constraint specifications. Secondly, GUARD has self-contained implementations of a comprehensive range of state-of-the-art safe RL algorithms. Lastly, GUARD is highly customizable, allowing researchers to tailor tasks and algorithms to specific needs. Using GUARD, we present a comparative analysis of state-of-the-art safe RL algorithms across various task settings, establishing essential baselines for future research.

## References

- Volodymyr Mnih, Koray Kavukcuoglu, David Silver, Alex Graves, Ioannis Antonoglou, Daan Wierstra, and Martin Riedmiller. Playing atari with deep reinforcement learning. *arXiv preprint arXiv:1312.5602*, 2013.
- Weiyue Zhao, Yang Liu, Xiaoming Zhao, J Qiu, and Jian Peng. Approximation gradient error variance reduced optimization. In *Workshop on Reinforcement Learning in Games (RLG) at The Thirty-Third AAAI Conference on Artificial Intelligence*, 2019a.
- David Silver, Thomas Hubert, Julian Schrittwieser, Ioannis Antonoglou, Matthew Lai, Arthur Guez, Marc Lanctot, Laurent Sifre, Dharshan Kumaran, Thore Graepel, et al. A general reinforcement learning algorithm that masters chess, shogi, and go through self-play. *Science*, 362(6419): 1140–1144, 2018.
- OpenAI, :, Christopher Berner, Greg Brockman, Brooke Chan, Vicki Cheung, Przemysław Dębiak, Christy Dennison, David Farhi, Quirin Fischer, Shariq Hashme, Chris Hesse, Rafal Józefowicz, Scott Gray, Catherine Olsson, Jakub Pachocki, Michael Petrov, Henrique P. d. O. Pinto, Jonathan Raiman, Tim Salimans, Jeremy Schlatter, Jonas Schneider, Szymon Sidor, Ilya Sutskever, Jie Tang, Filip Wolski, and Susan Zhang. Dota 2 with large scale deep reinforcement learning. *arXiv preprint arXiv:1912.06680*, 2019.
- Oriol Vinyals, Igor Babuschkin, Junyoung Chung, Michael Mathieu, Max Jaderberg, Wojtek Czarnecki, Andrew Dudzik, Aja Huang, Petko Georgiev, Richard Powell, Timo Ewalds, Dan Horgan, Manuel Kroiss, Ivo Danihelka, John Agapiou, Junhyuk Oh, Valentin Dalibard, David Choi, Laurent Sifre, Yury Sulsky, Sasha Vezhnevets, James Molloy, Trevor

- Cai, David Budden, Tom Paine, Caglar Gulcehre, Ziyu Wang, Tobias Pfaff, Toby Pohlen, Dani Yogatama, Julia Cohen, Katrina McKinney, Oliver Smith, Tom Schaul, Timothy Lillicrap, Chris Apps, Koray Kavukcuoglu, Demis Hassabis, and David Silver. AlphaStar: Mastering the Real-Time Strategy Game StarCraft II. <https://deepmind.com/blog/alphastar-mastering-real-time-strategy-game-starcraft-ii/>, 2019.
- Wei-Ye Zhao, Xi-Ya Guan, Yang Liu, Xiaoming Zhao, and Jian Peng. Stochastic variance reduction for deep q-learning. *arXiv preprint arXiv:1905.08152*, 2019b.
- Ivaylo Popov, Nicolas Heess, Timothy Lillicrap, Roland Hafner, Gabriel Barth-Maron, Matej Vecerik, Thomas Lampe, Yuval Tassa, Tom Erez, and Martin Riedmiller. Data-efficient deep reinforcement learning for dexterous manipulation. *arXiv preprint arXiv:1704.03073*, 2017.
- Weiyi Zhao, Suqin He, and Changliu Liu. Provably safe tolerance estimation for robot arms via sum-of-squares programming. *IEEE Control Systems Letters*, 6:3439–3444, 2022a.
- Rui Chen, Alvin Shek, and Changliu Liu. Robust and context-aware real-time collaborative robot handling via dynamic gesture commands. *IEEE Robotics and Automation Letters*, 2023.
- Forest Agostinelli, Stephen McAleer, Alexander Shmakov, and Pierre Baldi. Solving the rubik’s cube with deep reinforcement learning and search. *Nature Machine Intelligence*, pages 1–8, 2019.
- Alvin Shek, Rui Chen, and Changliu Liu. Learning from physical human feedback: An object-centric one-shot adaptation method. *arXiv preprint arXiv:2203.04951*, 2022.
- Wei-Ye Zhao, Suqin He, Chengtao Wen, and Changliu Liu. Contact-rich trajectory generation in confined environments using iterative convex optimization. In *Dynamic Systems and Control Conference*, volume 84287, page V002T31A002. American Society of Mechanical Engineers, 2020a.
- Charles Noren, Weiye Zhao, and Changliu Liu. Safe adaptation with multiplicative uncertainties using robust safe set algorithm. *IFAC-PapersOnLine*, 54(20):360–365, 2021.
- David Isele, Alireza Nakhaei, and Kikuo Fujimura. Safe reinforcement learning on autonomous vehicles. *arXiv preprint arXiv:1910.00399*, 2019.
- B Ravi Kiran, Ibrahim Sobh, Victor Talpaert, Patrick Mannion, Ahmad A. Al Sallab, Senthil Yogamani, and Patrick Pérez. Deep reinforcement learning for autonomous driving: A survey. *IEEE Transactions on Intelligent Transportation Systems*, 23(6):4909–4926, 2022.
- Shangding Gu, Guang Chen, Lijun Zhang, Jing Hou, Yingbai Hu, and Alois Knoll. Constrained reinforcement learning for vehicle motion planning with topological reachability analysis. *Robotics*, 11(4), 2022a.
- Jens Kober, J. Andrew Bagnell, and Jan Peters. Reinforcement learning in robotics: A survey. *The International Journal of Robotics Research*, 32(11):1238–1274, 2013.
- Lukas Brunke, Melissa Greeff, Adam W. Hall, Zhaocong Yuan, Siqi Zhou, Jacopo Panerati, and Angela P. Schoellig. Safe learning in robotics: From learning-based control to safe reinforcement learning. *Annual Review of Control, Robotics, and Autonomous Systems*, 5(1):411–444, 2022.
- Weiyi Zhao, Tairan He, Tianhao Wei, Simin Liu, and Changliu Liu. Safety index synthesis via sum-of-squares programming. *arXiv preprint arXiv:2209.09134*, 2022b.
- Weiyi Zhao, Liting Sun, Changliu Liu, and Masayoshi Tomizuka. Experimental evaluation of human motion prediction toward safe and efficient human robot collaboration. In *2020 American Control Conference (ACC)*, pages 4349–4354. IEEE, 2020b.
- Yifan Sun, Weiye Zhao, and Changliu Liu. Hybrid task constrained planner for robot manipulator in confined environment. *arXiv preprint arXiv:2304.09260*, 2023.
- Yujiao Cheng, Weiye Zhao, Changliu Liu, and Masayoshi Tomizuka. Human motion prediction using semi-adaptable neural networks. In *2019 American Control Conference (ACC)*, pages 4884–4890. IEEE, 2019.

- Javier Garcia and Fernando Fernández. A comprehensive survey on safe reinforcement learning. *Journal of Machine Learning Research*, 16(1):1437–1480, 2015.
- Shangding Gu, Long Yang, Yali Du, Guang Chen, Florian Walter, Jun Wang, Yaodong Yang, and Alois Knoll. A review of safe reinforcement learning: Methods, theory and applications. *arXiv preprint arXiv:2205.10330*, 2022b.
- Weiyi Zhao, Tairan He, Rui Chen, Tianhao Wei, and Changliu Liu. State-wise safe reinforcement learning: A survey. *The 32nd International Joint Conference on Artificial Intelligence (IJCAI)*, 2023.
- Weiyi Zhao, Tairan He, and Changliu Liu. Probabilistic safeguard for reinforcement learning using safety index guided gaussian process models. *arXiv preprint arXiv:2210.01041*, 2022c.
- Suqin He, Weiyi Zhao, Chuxiong Hu, Yu Zhu, and Changliu Liu. A hierarchical long short term safety framework for efficient robot manipulation under uncertainty. *Robotics and Computer-Integrated Manufacturing*, 82:102522, 2023a.
- Tianhao Wei, Shucheng Kang, Weiyi Zhao, and Changliu Liu. Persistently feasible robust safe control by safety index synthesis and convex semi-infinite programming. *IEEE Control Systems Letters*, 2022.
- Weiyi Zhao, Tairan He, and Changliu Liu. Model-free safe control for zero-violation reinforcement learning. In *5th Annual Conference on Robot Learning*, 2021.
- Tairan He, Weiyi Zhao, and Changliu Liu. Autocost: Evolving intrinsic cost for zero-violation reinforcement learning. *Proceedings of the AAAI Conference on Artificial Intelligence*, 2023b.
- Yan Duan, Xi Chen, Rein Houthooft, John Schulman, and Pieter Abbeel. Benchmarking deep reinforcement learning for continuous control. In *International conference on machine learning*, pages 1329–1338. PMLR, 2016.
- Greg Brockman, Vicki Cheung, Ludwig Pettersson, Jonas Schneider, John Schulman, Jie Tang, and Wojciech Zaremba. Openai gym. *arXiv preprint arXiv:1606.01540*, 2016.
- Benjamin Ellenberger. Pybullet gymperium. <https://github.com/benelot/pybullet-gym>, 2018–2019.
- Tianhe Yu, Deirdre Quillen, Zhanpeng He, Ryan Julian, Karol Hausman, Chelsea Finn, and Sergey Levine. Meta-world: A benchmark and evaluation for multi-task and meta reinforcement learning. In *Conference on Robot Learning (CoRL)*, 2019.
- Ian Osband, Yotam Doron, Matteo Hessel, John Aslanides, Eren Sezener, Andre Saraiva, Katrina McKinney, Tor Lattimore, Csaba Szepesvári, Satinder Singh, Benjamin Van Roy, Richard Sutton, David Silver, and Hado van Hasselt. Behaviour suite for reinforcement learning. In *International Conference on Learning Representations*, 2020.
- Saran Tunyasuvunakool, Alistair Muldal, Yotam Doron, Siqi Liu, Steven Bohez, Josh Merel, Tom Erez, Timothy Lillicrap, Nicolas Heess, and Yuval Tassa. dm\_control: Software and tasks for continuous control. *Software Impacts*, 6:100022, 2020.
- Gabriel Dulac-Arnold, Nir Levine, Daniel J. Mankowitz, Jerry Li, Cosmin Paduraru, Sven Gowal, and Todd Hester. An empirical investigation of the challenges of real-world reinforcement learning. 2020.
- Linrui Zhang, Qin Zhang, Li Shen, Bo Yuan, and Xueqian Wang. Saferl-kit: Evaluating efficient reinforcement learning methods for safe autonomous driving. *arXiv preprint arXiv:2206.08528*, 2022a.
- Alex Ray, Joshua Achiam, and Dario Amodei. Benchmarking safe exploration in deep reinforcement learning. *CoRR*, abs/1910.01708, 2019.
- Joshua Achiam. Spinning Up in Deep Reinforcement Learning. 2018.

- Joshua Achiam, David Held, Aviv Tamar, and Pieter Abbeel. Constrained policy optimization. In *International conference on machine learning*, pages 22–31. PMLR, 2017a.
- Sven Gronauer. Bullet-safety-gym: A framework for constrained reinforcement learning. Technical report, TUM Department of Electrical and Computer Engineering, Jan 2022.
- Jiayi Weng, Huayu Chen, Dong Yan, Kaichao You, Alexis Duburcq, Minghao Zhang, Yi Su, Hang Su, and Jun Zhu. Tianshou: A highly modularized deep reinforcement learning library. *Journal of Machine Learning Research*, 23(267):1–6, 2022. URL <http://jmlr.org/papers/v23/21-1127.html>.
- Antonin Raffin, Ashley Hill, Adam Gleave, Anssi Kanervisto, Maximilian Ernestus, and Noah Dormann. Stable-baselines3: Reliable reinforcement learning implementations. *Journal of Machine Learning Research*, 22(268):1–8, 2021. URL <http://jmlr.org/papers/v22/20-1364.html>.
- Eric Liang, Richard Liaw, Robert Nishihara, Philipp Moritz, Roy Fox, Ken Goldberg, Joseph E. Gonzalez, Michael I. Jordan, and Ion Stoica. RLlib: Abstractions for distributed reinforcement learning. In *International Conference on Machine Learning (ICML)*, 2018.
- Prafulla Dhariwal, Christopher Hesse, Oleg Klimov, Alex Nichol, Matthias Plappert, Alec Radford, John Schulman, Szymon Sidor, Yuhuai Wu, and Peter Zhokhov. Openai baselines. <https://github.com/openai/baselines>, 2017.
- Ashley Hill, Antonin Raffin, Maximilian Ernestus, Adam Gleave, Anssi Kanervisto, Rene Traore, Prafulla Dhariwal, Christopher Hesse, Oleg Klimov, Alex Nichol, Matthias Plappert, Alec Radford, John Schulman, Szymon Sidor, and Yuhuai Wu. Stable baselines. <https://github.com/hill-a/stable-baselines>, 2018.
- Pablo Samuel Castro, Subhodeep Moitra, Carles Gelada, Saurabh Kumar, and Marc G. Bellemare. Dopamine: A Research Framework for Deep Reinforcement Learning. 2018. URL <http://arxiv.org/abs/1812.06110>.
- Matthew W. Hoffman, Bobak Shahriari, John Aslanides, Gabriel Barth-Maron, Nikola Momchev, Danila Sinopalnikov, Piotr Stańczyk, Sabela Ramos, Anton Raichuk, Damien Vincent, Léonard Huszenot, Robert Dadashi, Gabriel Dulac-Arnold, Manu Orsini, Alexis Jacq, Johan Ferret, Nino Vieillard, Seyed Kamyar Seyed Ghasemipour, Sertan Girgin, Olivier Pietquin, Feryal Behbahani, Tamara Norman, Abbas Abdolmaleki, Albin Cassirer, Fan Yang, Kate Baumli, Sarah Henderson, Abe Friesen, Ruba Haroun, Alex Novikov, Sergio Gómez Colmenarejo, Serkan Cabi, Caglar Gulcehre, Tom Le Paine, Srivatsan Srinivasan, Andrew Cowie, Ziyu Wang, Bilal Piot, and Nando de Freitas. Acme: A research framework for distributed reinforcement learning. *arXiv preprint arXiv:2006.00979*, 2020. URL <https://arxiv.org/abs/2006.00979>.
- Matthias Plappert. keras-rl. <https://github.com/keras-rl/keras-rl>, 2016.
- Zhaocong Yuan, Adam W. Hall, Siqi Zhou, Lukas Brunke, Melissa Greeff, Jacopo Panerati, and Angela P. Schoellig. Safe-control-gym: A unified benchmark suite for safe learning-based control and reinforcement learning in robotics. *IEEE Robotics and Automation Letters*, 7(4):11142–11149, 2022. doi: 10.1109/LRA.2022.3196132.
- Steven Bohez, Abbas Abdolmaleki, Michael Neunert, Jonas Buchli, Nicolas Heess, and Raia Hadsell. Value constrained model-free continuous control. *arXiv preprint arXiv:1902.04623*, 2019.
- Haitong Ma, Yang Guan, Shegnbo Eben Li, Xiangteng Zhang, Sifa Zheng, and Jianyu Chen. Feasible actor-critic: Constrained reinforcement learning for ensuring statewise safety. *arXiv preprint arXiv:2105.10682*, 2021.
- Yongshuai Liu, Jiaxin Ding, and Xin Liu. Ipo: Interior-point policy optimization under constraints. In *Proceedings of the AAAI conference on artificial intelligence*, volume 34, pages 4940–4947, 2020.
- Tsung-Yen Yang, Justinian Rosca, Karthik Narasimhan, and Peter J Ramadge. Projection-based constrained policy optimization. *arXiv preprint arXiv:2010.03152*, 2020.

Gal Dalal, Krishnamurthy Dvijotham, Matej Vecerik, Todd Hester, Cosmin Paduraru, and Yuval Tassa. Safe exploration in continuous action spaces. *CoRR*, abs/1801.08757, 2018.

John Schulman, Sergey Levine, Pieter Abbeel, Michael Jordan, and Philipp Moritz. Trust region policy optimization. In *International conference on machine learning*, pages 1889–1897. PMLR, 2015.

Joshua Achiam, David Held, Aviv Tamar, and Pieter Abbeel. Constrained policy optimization. In *International Conference on Machine Learning*, pages 22–31. PMLR, 2017b.

Stephen P Boyd and Lieven Vandenberghe. *Convex optimization*. Cambridge university press, 2004.

Linrui Zhang, Qin Zhang, Li Shen, Bo Yuan, Xueqian Wang, and Dacheng Tao. Evaluating model-free reinforcement learning toward safety-critical tasks. *arXiv preprint arXiv:2212.05727*, 2022b.

## Checklist

1. For all authors...
  - (a) Do the main claims made in the abstract and introduction accurately reflect the paper's contributions and scope? **[Yes]** Both abstract and introduction emphasize the environment and algorithm implementation.
  - (b) Did you describe the limitations of your work? **[Yes]** See Section 4.1, we only consider model-free safe RL algorithms.
  - (c) Did you discuss any potential negative societal impacts of your work? **[No]** We don't anticipate any negative societal impacts of our work.
  - (d) Have you read the ethics review guidelines and ensured that your paper conforms to them? **[Yes]** We have read the guidelines and ensured our paper conforms to them.
2. If you are including theoretical results...
  - (a) Did you state the full set of assumptions of all theoretical results? **[N/A]** This paper doesn't introduce new theoretical results.
  - (b) Did you include complete proofs of all theoretical results? **[N/A]** This paper doesn't introduce new theoretical results.
3. If you ran experiments (e.g. for benchmarks)...
  - (a) Did you include the code, data, and instructions needed to reproduce the main experimental results (either in the supplemental material or as a URL)? **[Yes]** See Appendix B, the full instructions and code can be found in the listed URL.
  - (b) Did you specify all the training details (e.g., data splits, hyperparameters, how they were chosen)? **[Yes]** See Appendix B.
  - (c) Did you report error bars (e.g., with respect to the random seed after running experiments multiple times)? **[Yes]** See Figures 6 to 10.
  - (d) Did you include the total amount of compute and the type of resources used (e.g., type of GPUs, internal cluster, or cloud provider)? **[Yes]** See Appendix B.1.
4. If you are using existing assets (e.g., code, data, models) or curating/releasing new assets...
  - (a) If your work uses existing assets, did you cite the creators? **[Yes]** See Section 1, where we mentioned that our work is based on Safety Gym, and SpinningUp.
  - (b) Did you mention the license of the assets? **[Yes]** See Appendix B, we mentioned the license of the codebases that inspire our implementation.
  - (c) Did you include any new assets either in the supplemental material or as a URL? **[Yes]** See Appendix B, the full code can be found in the URL.
  - (d) Did you discuss whether and how consent was obtained from people whose data you're using/curating? **[N/A]** We don't introduce new dataset.
  - (e) Did you discuss whether the data you are using/curating contains personally identifiable information or offensive content? **[N/A]** We don't introduce new dataset.
5. If you used crowdsourcing or conducted research with human subjects...
  - (a) Did you include the full text of instructions given to participants and screenshots, if applicable? **[N/A]** Our work doesn't include human subjects.
  - (b) Did you describe any potential participant risks, with links to Institutional Review Board (IRB) approvals, if applicable? **[N/A]** Our work doesn't include human subjects.
  - (c) Did you include the estimated hourly wage paid to participants and the total amount spent on participant compensation? **[N/A]** Our work doesn't include human subjects.

## A Environment Details

### A.1 Observation Space and Action space of different robots

The action space and observation space of different robots are summarized in Tables 1 to 16

Table 1: Action space of Swimmer

Num	Action	Min	Max	Name in XML	Joint	Unit
0	Torque applied on the first rotor	-1	1	motor1_rot	hinge	torque (Nm)
1	Torque applied on the second rotor	-1	1	motor2_rot	hinge	torque (Nm)

Table 2: Observation space of Swimmer

Num	Observation	Min	Max	Name in XML	Joint	Unit
0/1/2	3-axis linear acceleration of the torso (including gravity)	-Inf	Inf	accelerometer	free	acceleration ( $m/s^2$ )
3/4/5	3-axis linear velocity of the torso	-Inf	Inf	velocimeter	free	velocity ( $m/s$ )
6/7/8	3-axis angular velocity velocity of the torso	-Inf	Inf	gyro	free	angular velocity ( $rad/s$ )
9/10/11	3D magnetic flux vector at the torso	-Inf	Inf	magnetometer	free	magnetic flux density ( $T$ )
12	Contact force at the first tip	0	Inf	touch_point1	-	force(N)
13	Contact force at the first rotor	0	Inf	touch_point2	-	force(N)
14	Contact force at the second rotor	0	Inf	touch_point3	-	force(N)
15	Contact force at the second tip	0	Inf	touch_point4	-	force(N)
16	Angle of the first rotor	-Inf	Inf	jointpos_motor1_rot	hinge	angle (rad)
17	Angle of the second rotor	-Inf	Inf	jointpos_motor2_rot	hinge	angle (rad)
18	Angular velocity of the first rotor	-Inf	Inf	jointvel_motor1_rot	hinge	angular velocity ( $rad/s$ )
19	Angular velocity of the second rotor	-Inf	Inf	jointvel_motor2_rot	hinge	angular velocity ( $rad/s$ )

Table 3: Action space of Ant

Num	Action	Min	Max	Name in XML	Joint	Unit
0	Torque applied on the rotor between the torso and front left hip	-1	1	hip_1	hinge	torque (Nm)
1	Torque applied on the rotor between the front left two links	-1	1	ankle_1	hinge	torque (Nm)
2	Torque applied on the rotor between the torso and front right hip	-1	1	hip_2	hinge	torque (Nm)
3	Torque applied on the rotor between the front right two links	-1	1	ankle_2	hinge	torque (Nm)
4	Torque applied on the rotor between the torso and back left hip	-1	1	hip_3	hinge	torque (Nm)
5	Torque applied on the rotor between the back left two links	-1	1	ankle_3	hinge	torque (Nm)
6	Torque applied on the rotor between the torso and back right hip	-1	1	hip_4	hinge	torque (Nm)
7	Torque applied on the rotor between the back right two links	-1	1	ankle_4	hinge	torque (Nm)

Table 4: Observation space of Ant

Num	Observation	Min	Max	Name in XML	Joint	Unit
0/1/2	3-axis linear acceleration of the torso (including gravity)	-Inf	Inf	accelerometer	free	acceleration ( $m/s^2$ )
3/4/5	3-axis linear velocity of the torso	-Inf	Inf	velocity	free	velocity ( $m/s$ )
6/7/8	3-axis angular velocity of the torso	-Inf	Inf	gyro	free	angular velocity ( $rad/s$ )
9/10/11	3D magnetic flux vector at the torso	-Inf	Inf	magnetometer	free	magnetic flux density ( $T$ )
12	Contact force at the front left ankle	0	Inf	touch_ankle_1a	-	force(N)
13	Contact force at the front right ankle	0	Inf	touch_ankle_2a	-	force(N)
14	Contact force at the back left ankle	0	Inf	touch_ankle_3a	-	force(N)
15	Contact force at the back left ankle	0	Inf	touch_ankle_4a	-	force(N)
16	Contact force at the end of the front left leg	0	Inf	touch_ankle_1b	-	force(N)
17	Contact force at the end of the front right leg	0	Inf	touch_ankle_2b	-	force(N)
18	Contact force at the end of the back left leg	0	Inf	touch_ankle_3b	-	force(N)
19	Contact force at the end of the back left leg	0	Inf	touch_ankle_4b	-	force(N)
20	Angle of the front left hip	-Inf	Inf	jointpos_hip_1	hinge	angle (rad)
21	Angle of the front right hip	-Inf	Inf	jointpos_hip_2	hinge	angle (rad)
22	Angle of the back left hip	-Inf	Inf	jointpos_hip_3	hinge	angle (rad)
23	Angle of the back right hip	-Inf	Inf	jointpos_hip_4	hinge	angle (rad)
24	Angle of the front left ankle	-Inf	Inf	jointpos_ankle_1	hinge	angle (rad)
25	Angle of the front right ankle	-Inf	Inf	jointpos_ankle_2	hinge	angle (rad)
26	Angle of the back left ankle	-Inf	Inf	jointpos_ankle_3	hinge	angle (rad)
27	Angle of the back right ankle	-Inf	Inf	jointpos_ankle_4	hinge	angle (rad)
28	Angular velocity of the front left hip	-Inf	Inf	jointvel_hip_1	hinge	angular velocity ( $rad/s$ )
29	Angular velocity of the front right hip	-Inf	Inf	jointvel_hip_2	hinge	angular velocity ( $rad/s$ )
30	Angular velocity of the back left hip	-Inf	Inf	jointvel_hip_3	hinge	angular velocity ( $rad/s$ )
31	Angular velocity of the back right hip	-Inf	Inf	jointvel_hip_4	hinge	angular velocity ( $rad/s$ )
32	Angular velocity of the front left ankle	-Inf	Inf	jointvel_ankle_1	hinge	angular velocity ( $rad/s$ )
33	Angular velocity of the front right ankle	-Inf	Inf	jointvel_ankle_2	hinge	angular velocity ( $rad/s$ )
34	Angular velocity of the back left ankle	-Inf	Inf	jointvel_ankle_3	hinge	angular velocity ( $rad/s$ )
35	Angular velocity of the back right ankle	-Inf	Inf	jointvel_ankle_4	hinge	angular velocity ( $rad/s$ )

Table 5: Action space of Walker

Num	Action	Min	Max	Name in XML	Joint	Unit
0	Torque applied on the rotor between torso and the right hip (x-coordinate)	-1	1	right_hip_x	hinge	torque (Nm)
1	Torque applied on the rotor between torso and the right hip (z-coordinate)	-1	1	right_hip_z	hinge	torque (Nm)
2	Torque applied on the rotor between torso and the right hip (y-coordinate)	-1	1	right_hip_y	hinge	torque (Nm)
3	Torque applied on the right leg rotor	-1	1	right_leg_joint	hinge	torque (Nm)
4	Torque applied on the right foot rotor	-1	1	right_foot_joint	hinge	torque (Nm)
5	Torque applied on the rotor between torso and the left hip (x-coordinate)	-1	1	left_hip_x	hinge	torque (Nm)
6	Torque applied on the rotor between torso and the left hip (z-coordinate)	-1	1	left_hip_z	hinge	torque (Nm)
7	Torque applied on the rotor between torso and the left hip (y-coordinate)	-1	1	left_hip_y	hinge	torque (Nm)
8	Torque applied on the left leg rotor	-1	1	left_leg_joint	hinge	torque (Nm)
9	Torque applied on the left foot rotor	-1	1	left_foot_joint	hinge	torque (Nm)

Table 6: Observation space of Walker

Num	Observation	Min	Max	Name in XML	Joint	Unit
0/1/2	3-axis linear acceleration of the torso (including gravity)	-Inf	Inf	accelerometer	free	acceleration ( $m/s^2$ )
3/4/5	3-axis linear velocity of the torso	-Inf	Inf	velocity	free	velocity ( $m/s$ )
6/7/8	3-axis angular velocity of the torso	-Inf	Inf	gyro	free	angular velocity ( $rad/s$ )
9/10/11	3D magnetic flux vector at the torso	-Inf	Inf	magnetometer	free	magnetic flux density ( $T$ )
12	Contact force at the right foot	0	Inf	touch_right_foot	-	force( $N$ )
13	Contact force at the left foot	0	Inf	touch_left_foot	-	force( $N$ )
14	Angle of the right hip (x-coordinate)	-Inf	Inf	jointpos_right_hip_x	hinge	angle ( $rad$ )
15	Angle of the right hip (z-coordinate)	-Inf	Inf	jointpos_right_hip_z	hinge	angle ( $rad$ )
16	Angle of the right hip (y-coordinate)	-Inf	Inf	jointpos_right_hip_y	hinge	angle ( $rad$ )
17	Angle of the right leg	-Inf	Inf	jointpos_right_leg	hinge	angle ( $rad$ )
18	Angle of the right foot	-Inf	Inf	jointpos_right_foot	hinge	angle ( $rad$ )
19	Angle of the left hip (x-coordinate)	-Inf	Inf	jointpos_left_hip_x	hinge	angle ( $rad$ )
20	Angle of the left hip (z-coordinate)	-Inf	Inf	jointpos_left_hip_z	hinge	angle ( $rad$ )
21	Angle of the left hip (y-coordinate)	-Inf	Inf	jointpos_left_hip_y	hinge	angle ( $rad$ )
22	Angle of the left leg	-Inf	Inf	jointpos_left_leg	hinge	angle ( $rad$ )
23	Angle of the left foot	-Inf	Inf	jointpos_left_foot	hinge	angle ( $rad$ )
24	Angular velocity of the right hip (x-coordinate)	-Inf	Inf	jointvel_right_hip_x	hinge	angular velocity ( $rad/s$ )
25	Angular velocity of the right hip (z-coordinate)	-Inf	Inf	jointvel_right_hip_z	hinge	angular velocity ( $rad/s$ )
26	Angular velocity of the right hip (y-coordinate)	-Inf	Inf	jointvel_right_hip_y	hinge	angular velocity ( $rad/s$ )
27	Angular velocity of the right leg	-Inf	Inf	jointvel_right_leg	hinge	angular velocity ( $rad/s$ )
28	Angular velocity of the right foot	-Inf	Inf	jointvel_right_foot	hinge	angular velocity ( $rad/s$ )
29	Angular velocity of the left hip (x-coordinate)	-Inf	Inf	jointvel_left_hip_x	hinge	angular velocity ( $rad/s$ )
30	Angular velocity of the left hip (z-coordinate)	-Inf	Inf	jointvel_left_hip_z	hinge	angular velocity ( $rad/s$ )
31	Angular velocity of the left hip (y-coordinate)	-Inf	Inf	jointvel_left_hip_y	hinge	angular velocity ( $rad/s$ )
32	Angular velocity of the left leg	-Inf	Inf	jointvel_left_leg	hinge	angular velocity ( $rad/s$ )
33	Angular velocity of the left foot	-Inf	Inf	jointvel_left_foot	hinge	angular velocity ( $rad/s$ )

Table 7: Action space of Humanoid

Num	Action	Min	Max	Name in XML	Joint	Unit
0	Torque applied on the rotor between torso and the right hip (x-coordinate)	-1	1	right_hip_x	hinge	torque (Nm)
1	Torque applied on the rotor between torso and the right hip (z-coordinate)	-1	1	right_hip_z	hinge	torque (Nm)
2	Torque applied on the rotor between torso and the right hip (y-coordinate)	-1	1	right_hip_y	hinge	torque (Nm)
3	Torque applied on the right knee rotor	-1	1	right_knee	hinge	torque (Nm)
4	Torque applied on the rotor between torso and the left hip (x-coordinate)	-1	1	left_hip_x	hinge	torque (Nm)
5	Torque applied on the rotor between torso and the left hip (z-coordinate)	-1	1	left_hip_z	hinge	torque (Nm)
6	Torque applied on the rotor between torso and the left hip (y-coordinate)	-1	1	left_hip_y	hinge	torque (Nm)
7	Torque applied on the left knee rotor	-1	1	left_knee	hinge	torque (Nm)

Table 8: Observation space of Humanoid

Num	Observation	Min	Max	Name in XML	Joint	Unit
0/1/2	3-axis linear acceleration of the torso (including gravity)	-Inf	Inf	accelerometer	free	acceleration ( $m/s^2$ )
3/4/5	3-axis linear velocity of the torso	-Inf	Inf	velocity	free	velocity ( $m/s$ )
6/7/8	3-axis angular velocity of the torso	-Inf	Inf	gyro	free	angular velocity ( $rad/s$ )
9/10/11	3D magnetic flux vector at the torso	-Inf	Inf	magnetometer	free	magnetic flux density ( $T$ )
12	Contact force at the right foot	0	Inf	touch_right_foot	-	force(N)
13	Contact force at the left foot	0	Inf	touch_left_foot	-	force(N)
14	Angle of the right hip (x-coordinate)	-Inf	Inf	jointpos_right_hip_x	hinge	angle (rad)
15	Angle of the right hip (z-coordinate)	-Inf	Inf	jointpos_right_hip_z	hinge	angle (rad)
16	Angle of the right hip (y-coordinate)	-Inf	Inf	jointpos_right_hip_y	hinge	angle (rad)
17	Angle of the right knee	-Inf	Inf	jointpos_right_knee	hinge	angle (rad)
18	Angle of the left hip (x-coordinate)	-Inf	Inf	jointpos_left_hip_x	hinge	angle (rad)
19	Angle of the left hip (z-coordinate)	-Inf	Inf	jointpos_left_hip_z	hinge	angle (rad)
20	Angle of the left hip (y-coordinate)	-Inf	Inf	jointpos_left_hip_y	hinge	angle (rad)
21	Angle of the left leg	-Inf	Inf	jointpos_left_knee	hinge	angle (rad)
22	Angular velocity of the right hip (x-coordinate)	-Inf	Inf	jointvel_right_hip_x	hinge	angular velocity ( $rad/s$ )
23	Angular velocity of the right hip (z-coordinate)	-Inf	Inf	jointvel_right_hip_z	hinge	angular velocity ( $rad/s$ )
24	Angular velocity of the right hip (y-coordinate)	-Inf	Inf	jointvel_right_hip_y	hinge	angular velocity ( $rad/s$ )
25	Angular velocity of the right knee	-Inf	Inf	jointvel_right_knee	hinge	angular velocity ( $rad/s$ )
26	Angular velocity of the left hip (x-coordinate)	-Inf	Inf	jointvel_left_hip_x	hinge	angular velocity ( $rad/s$ )
27	Angular velocity of the left hip (z-coordinate)	-Inf	Inf	jointvel_left_hip_z	hinge	angular velocity ( $rad/s$ )
28	Angular velocity of the left hip (y-coordinate)	-Inf	Inf	jointvel_left_hip_y	hinge	angular velocity ( $rad/s$ )
29	Angular velocity of the left knee	-Inf	Inf	jointvel_left_knee	hinge	angular velocity ( $rad/s$ )

Table 9: Action space of Hopper

Num	Action	Min	Max	Name in XML	Joint	Unit
0	Torque applied on the rotor between torso and the hip (x-coordinate)	-1	1	hip_x	hinge	torque (Nm)
1	Torque applied on the rotor between torso and the hip (z-coordinate)	-1	1	hip_z	hinge	torque (Nm)
2	Torque applied on the rotor between torso and the hip (y-coordinate)	-1	1	hip_y	hinge	torque (Nm)
3	Torque applied on the thigh rotor	-1	1	thigh_joint	hinge	torque (Nm)
4	Torque applied on the leg rotor	-1	1	leg_joint	hinge	torque (Nm)
5	Torque applied on the foot rotor	-1	1	foot_joint	hinge	torque (Nm)

Table 10: Observation space of Hopper

Num	Observation	Min	Max	Name in XML	Joint	Unit
0/1/2	3-axis linear acceleration of the torso (including gravity)	-Inf	Inf	accelerometer	free	acceleration ( $m/s^2$ )
3/4/5	3-axis linear velocity of the torso	-Inf	Inf	velocimeter	free	velocity ( $m/s$ )
6/7/8	3-axis angular velocity of the torso	-Inf	Inf	gyro	free	angular velocity ( $rad/s$ )
9/10/11	3D magnetic flux vector at the torso	-Inf	Inf	magnetometer	free	magnetic flux density ( $T$ )
12	Contact force at the foot	0	Inf	touch_foot	-	force(N)
13	Angle of the hip (x-coordinate)	-Inf	Inf	jointpos_hip_x	hinge	angle (rad)
14	Angle of the hip (z-coordinate)	-Inf	Inf	jointpos_hip_z	hinge	angle (rad)
15	Angle of the hip (y-coordinate)	-Inf	Inf	jointpos_hip_y	hinge	angle (rad)
16	Angle of the thigh	-Inf	Inf	jointpos_thigh	hinge	angle (rad)
17	Angle of the leg	-Inf	Inf	jointpos_leg	hinge	angle (rad)
18	Angle of the foot	-Inf	Inf	jointpos_foot	hinge	angle (rad)
19	Angular velocity of the hip (x-coordinate)	-Inf	Inf	jointvel_hip_x	hinge	angular velocity ( $rad/s$ )
20	Angular velocity of the hip (z-coordinate)	-Inf	Inf	jointvel_hip_z	hinge	angular velocity ( $rad/s$ )
21	Angular velocity of the hip (y-coordinate)	-Inf	Inf	jointvel_hip_y	hinge	angular velocity ( $rad/s$ )
22	Angular velocity of the thigh	-Inf	Inf	jointvel_thigh	hinge	angular velocity ( $rad/s$ )
23	Angular velocity of the leg	-Inf	Inf	jointvel_leg	hinge	angular velocity ( $rad/s$ )
24	Angular velocity of the foot	-Inf	Inf	jointvel_foot	hinge	angular velocity ( $rad/s$ )

Table 11: Action space of Arm3

Num	Action	Min	Max	Name in XML	Joint	Unit
0	Torque applied on the first joint (connecting the base point and the first link)	-1	1	joint_1	hinge	torque (Nm)
1	Torque applied on the second joint(connecting the first and the second link)	-1	1	joint_2	hinge	torque (Nm)
2	Torque applied on the third joint (connecting the second and the third link)	-1	1	joint_3	hinge	torque (Nm)

Table 12: Observation space of Arm3

Num	Observation	Min	Max	Name in XML	Joint	Unit
0/1/2	3-axis linear acceleration of the first link (including gravity) 3-axis linear velocity of the first link	-Inf	Inf	accelerometer_link_1	free	acceleration ( $m/s^2$ )
3/4/5	3-axis angular velocity of the first link	-Inf	Inf	velocimeter_link_1	free	velocity ( $m/s$ )
6/7/8	3D magnetic flux vector at the first link	-Inf	Inf	gyro_link_1	free	angular velocity ( $rad/s$ )
9/10/11	3D magnetic flux vector of the first link	-Inf	Inf	magnetometer_link_1	free	magnetic flux density ( $T$ )
12/13/14	3-axis linear acceleration of the second link (including gravity)	-Inf	Inf	accelerometer_link_2	free	acceleration ( $m/s^2$ )
15/16/17	3-axis linear velocity of the second link	-Inf	Inf	velocimeter_link_2	free	velocity ( $m/s$ )
18/19/20	3-axis angular velocity of the second link	-Inf	Inf	gyro_link_2	free	angular velocity ( $rad/s$ )
21/22/23	3D magnetic flux vector at the second link	-Inf	Inf	magnetometer_link_2	free	magnetic flux density ( $T$ )
24/25/26	3-axis linear acceleration of the third link (including gravity)	-Inf	Inf	accelerometer_link_3	free	acceleration ( $m/s^2$ )
27/28/29	3-axis linear velocity of the third link	-Inf	Inf	velocimeter_link_3	free	velocity ( $m/s$ )
30/31/32	3-axis angular velocity velocity of the third link	-Inf	Inf	gyro_link_3	free	angular velocity ( $rad/s$ )
33/34/35	3D magnetic flux vector at the third link	-Inf	Inf	magnetometer_link_3	free	magnetic flux density ( $T$ )
36/37/38	3-axis linear acceleration of the fourth link (including gravity)	-Inf	Inf	accelerometer_link_4	free	acceleration ( $m/s^2$ )
39/40/41	3-axis linear velocity of the fourth link	-Inf	Inf	velocimeter_link_4	free	velocity ( $m/s$ )
42/43/44	3-axis angular velocity velocity of the fourth link	-Inf	Inf	gyro_link_4	free	angular velocity ( $rad/s$ )
45/46/47	3D magnetic flux vector at the fourth link	-Inf	Inf	magnetometer_link_4	free	magnetic flux density ( $T$ )
48/49/50	3-axis linear acceleration of the fifth link (including gravity)	-Inf	Inf	accelerometer_link_5	free	acceleration ( $m/s^2$ )
51/52/53	3-axis linear velocity of the fifth link	-Inf	Inf	velocimeter_link_5	free	velocity ( $m/s$ )
54/55/56	3-axis angular velocity velocity of the fifth link	-Inf	Inf	gyro_link_5	free	angular velocity ( $rad/s$ )
57/58/59	3D magnetic flux vector at the fifth link	-Inf	Inf	magnetometer_link_5	free	magnetic flux density ( $T$ )
60	Angle of the first joint	-Inf	Inf	jointpos_joint_1	hinge	angle ( $rad$ )
61	Angle of the second joint	-Inf	Inf	jointpos_joint_2	hinge	angle ( $rad$ )
62	Angle of the third joint	-Inf	Inf	jointpos_joint_3	hinge	angle ( $rad$ )
63	Angular velocity of the first joint	-Inf	Inf	jointvel_joint_1	hinge	angular velocity ( $rad/s$ )
64	Angular velocity of the second joint	-Inf	Inf	jointvel_joint_2	hinge	angular velocity ( $rad/s$ )
65	Angular velocity of the third joint	-Inf	Inf	jointvel_joint_3	hinge	angular velocity ( $rad/s$ )
66	Contact force at the end effector	0	Inf	touch_end_effector	-	force(N)

Table 13: Action space of Arm6

Num	Action	Min	Max	Name in XML	Joint	Unit
0	Torque applied on the first joint (connecting the base point and the first link)	-1	1	joint_1	hinge	torque ( $Nm$ )
1	Torque applied on the second joint(connecting the first and the second link)	-1	1	joint_2	hinge	torque ( $Nm$ )
2	Torque applied on the third joint (connecting the second and the third link)	-1	1	joint_3	hinge	torque ( $Nm$ )
3	Torque applied on the fourth joint (connecting the third and the fourth link)	-1	1	joint_4	hinge	torque ( $Nm$ )
4	Torque applied on the fifth joint (connecting the fourth and the fifth link)	-1	1	joint_5	hinge	torque ( $Nm$ )
5	Torque applied on the sixth joint (connecting the fifth and the sixth link)	-1	1	joint_6	hinge	torque ( $Nm$ )

Table 14: Observation space of Arm6

Num	Observation	Min	Max	Name in XML	Joint	Unit
0/1/2	3-axis linear acceleration of the first link (including gravity)	-Inf	Inf	accelerometer_link_1	free	acceleration ( $m/s^2$ )
3/4/5	3-axis linear velocity of the first link	-Inf	Inf	velocimeter_link_1	free	velocity ( $m/s$ )
6/7/8	3-axis angular velocity vector of the first link	-Inf	Inf	gyro_link_1	free	angular velocity ( $rad/s$ )
9/10/11	3D magnetic flux vector at the first link	-Inf	Inf	magnetometer_link_1	free	magnetic flux density ( $T$ )
12/13/14	3-axis linear acceleration of the second link (including gravity)	-Inf	Inf	accelerometer_link_2	free	acceleration ( $m/s^2$ )
15/16/17	3-axis linear velocity of the second link	-Inf	Inf	velocimeter_link_2	free	velocity ( $m/s$ )
18/19/20	3-axis angular velocity vector of the second link	-Inf	Inf	gyro_link_2	free	angular velocity ( $rad/s$ )
21/22/23	3D magnetic flux vector at the second link	-Inf	Inf	magnetometer_link_2	free	magnetic flux density ( $T$ )
24/25/26	3-axis linear acceleration of the third link (including gravity)	-Inf	Inf	accelerometer_link_3	free	acceleration ( $m/s^2$ )
27/28/29	3-axis linear velocity of the third link	-Inf	Inf	velocimeter_link_3	free	velocity ( $m/s$ )
30/31/32	3-axis angular velocity vector of the third link	-Inf	Inf	gyro_link_3	free	angular velocity ( $rad/s$ )
33/34/35	3D magnetic flux vector at the third link	-Inf	Inf	magnetometer_link_3	free	magnetic flux density ( $T$ )
36/37/38	3-axis linear acceleration of the fourth link (including gravity)	-Inf	Inf	accelerometer_link_4	free	acceleration ( $m/s^2$ )
39/40/41	3-axis linear velocity of the fourth link	-Inf	Inf	velocimeter_link_4	free	velocity ( $m/s$ )
42/43/44	3-axis angular velocity vector of the fourth link	-Inf	Inf	gyro_link_4	free	angular velocity ( $rad/s$ )
45/46/47	3D magnetic flux vector at the fourth link	-Inf	Inf	magnetometer_link_4	free	magnetic flux density ( $T$ )
48/49/50	3-axis linear acceleration of the fifth link (including gravity)	-Inf	Inf	accelerometer_link_5	free	acceleration ( $m/s^2$ )
51/52/53	3-axis linear velocity of the fifth link	-Inf	Inf	velocimeter_link_5	free	velocity ( $m/s$ )
54/55/56	3-axis angular velocity vector of the fifth link	-Inf	Inf	gyro_link_5	free	angular velocity ( $rad/s$ )
57/58/59	3D magnetic flux vector at the fifth link	-Inf	Inf	magnetometer_link_5	free	magnetic flux density ( $T$ )
60/61/62	3-axis linear acceleration of the sixth link (including gravity)	-Inf	Inf	accelerometer_link_6	free	acceleration ( $m/s^2$ )
63/64/65	3-axis linear velocity of the sixth link	-Inf	Inf	velocimeter_link_6	free	velocity ( $m/s$ )
66/67/68	3-axis angular velocity vector of the sixth link	-Inf	Inf	gyro_link_6	free	angular velocity ( $rad/s$ )
69/70/71	3D magnetic flux vector at the sixth link	-Inf	Inf	magnetometer_link_6	free	magnetic flux density ( $T$ )
72/73/74	3-axis linear acceleration of the seventh link (including gravity)	-Inf	Inf	accelerometer_link_7	free	acceleration ( $m/s^2$ )
75/76/77	3-axis linear velocity of the seventh link	-Inf	Inf	velocimeter_link_7	free	velocity ( $m/s$ )
78/79/80	3-axis angular velocity vector of the seventh link	-Inf	Inf	gyro_link_7	free	angular velocity ( $rad/s$ )
81/82/83	3D magnetic flux vector at the seventh link	-Inf	Inf	magnetometer_link_7	free	magnetic flux density ( $T$ )
84	Angle of the first joint	-Inf	Inf	jointpos_joint_1	hinge	angle ( $rad$ )
85	Angle of the second joint	-Inf	Inf	jointpos_joint_2	hinge	angle ( $rad$ )
86	Angle of the third joint	-Inf	Inf	jointpos_joint_3	hinge	angle ( $rad$ )
87	Angle of the fourth joint	-Inf	Inf	jointpos_joint_4	hinge	angle ( $rad$ )
88	Angle of the fifth joint	-Inf	Inf	jointpos_joint_5	hinge	angle ( $rad$ )
89	Angle of the sixth joint	-Inf	Inf	jointpos_joint_6	hinge	angle ( $rad$ )
90	Angular velocity of the first joint	-Inf	Inf	jointvel_joint_1	hinge	angular velocity ( $rad/s$ )
91	Angular velocity of the second joint	-Inf	Inf	jointvel_joint_2	hinge	angular velocity ( $rad/s$ )
92	Angular velocity of the third joint	-Inf	Inf	jointvel_joint_3	hinge	angular velocity ( $rad/s$ )
93	Angular velocity of the fourth joint	-Inf	Inf	jointvel_joint_4	hinge	angular velocity ( $rad/s$ )
94	Angular velocity of the fifth joint	-Inf	Inf	jointvel_joint_5	hinge	angular velocity ( $rad/s$ )
95	Angular velocity of the sixth joint	-Inf	Inf	jointvel_joint_6	hinge	angular velocity ( $rad/s$ )
96	Contact force at the end effector	0	0	touch_end_effector	-	force( $N$ )

Table 15: Action space of Drone

Num	Action	Min	Max	Name in XML	Joint	Unit
0	Extra thrust force applied on the first propeller	-1	1	-	-	force (N)
1	Extra thrust force applied on the second propeller	-1	1	-	-	force (N)
2	Extra thrust force applied on the third propeller	-1	1	-	-	force (N)
3	Extra thrust force applied on the fourth propeller	-1	1	-	-	force (N)

Table 16: Observation space of Drone

Num	Observation	Min	Max	Name in XML	Joint	Unit
0/1/2	3-axis linear acceleration of the torso (including gravity) 3-axis linear velocity of the torso 3-axis angular velocity velocity of the torso	-Inf	Inf	accelerometer velocity gyro	free free free	acceleration ( $m/s^2$ ) velocity ( $m/s$ ) angular velocity ( $rad/s$ )
3/4/5	3D magnetic flux vector at the torso	-Inf	Inf	magnetometer	free	magnetic flux density ( $T$ )
6/7/8	Contact force at the upper point of the first propeller Contact force at the lower point of the first propeller Contact force at the upper point of the second propeller	0	Inf	touch_p1a touch_p1b touch_p2a	- - -	force(N) force(N) force(N)
9/10/11	Contact force at the lower point of the second propeller Contact force at the upper point of the third propeller Contact force at the lower point of the third propeller Contact force at the upper point of the fourth propeller	0	Inf	touch_p2b touch_p3a touch_p3b touch_p4a	- - - -	force(N) force(N) force(N) force(N)
12	Contact force at the lower point of the fourth propeller	0	Inf	touch_p4b	-	force(N)
13						
14						
15						
16						
17						
18						
19						

## A.2 Observation Space Options and Desiderata

The observation spaces are also updated to match the new 3D tasks. The 3D compasses and 3D pseudo-lidars are introduced for 3D robots to sensor the position of targets in 3D space. Different from the single lidar system of the original environment, the Advanced Safety Gym allows to apply multiple lidars on different parts of the robot. For example, in Figure 5a the Arm robot is equipped with a 3D lidar and a 3D compass on each joint to obtain more environment information. Figure 5b shows a drone equipped with two 3D lidars to observe the 3D hazards and the 3D goal. The “lidar halos” of two lidars are distributed on two sphere with different radius. The number of “lidar halos” is configurable for more dense observations.

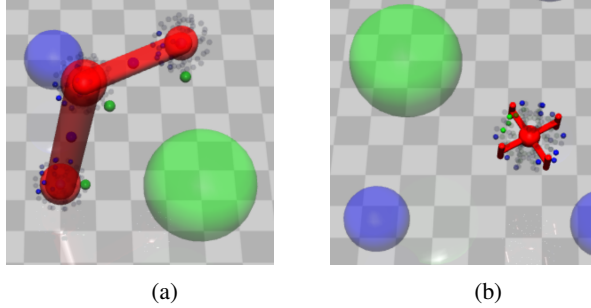


Figure 5: Visualizations of observation spaces

## A.3 Layout Randomization Options and Desiderata

The layout randomization is inherited from the original Safety Gym. In order to generate 3D objects, the  $z$  coordinate can be configured or randomly picked after the  $x$  and  $y$  coordinates are generated.

## A.4 Task and Constraint Details

Table 17: Comparison between different tasks

	GUARD Tasks				SafetyGym Tasks		
	Goal	Push	Chase	Defense	Goal	Button	Push
Interactive task		✓	✓	✓			✓
Non-interactive task	✓				✓	✓	
Contact task		✓	✓	✓		✓	✓
Non-contact task	✓		✓	✓	✓		
2D task	✓	✓	✓	✓	✓	✓	✓
3D task	✓		✓	✓			
Movable target		✓	✓	✓			✓
Immovable target	✓				✓	✓	
Single target	✓	✓	✓	✓	✓	✓	✓
Multiple targets			✓	✓			
General contact target	✓	✓	✓	✓			

Table 18: Comparison between different constraints

	New Constraints			Inherited Constraints				
	Ghosts	Ghosts 3D	Hazards 3D	Hazards	Vases	Pillars	Buttons	Gremlins
Trespassable	✓	✓			✓	✓	✓	✓
Untrespassable	✓	✓	✓	✓				
Immovable			✓	✓		✓	✓	
Passively movable					✓			
Actively movable	✓	✓						✓
3D motion		✓	✓					
2D motion	✓	✓	✓	✓	✓	✓	✓	✓

## A.5 Dynamics of movable objects

We begin by defining the distance vector  $d_{\text{origin}} = x_{\text{origin}} - x_{\text{object}}$ , which represents the distance from the position of the dynamic object  $x_{\text{object}}$  to the origin point of the world framework  $x_{\text{origin}}$ . By default, the origin point is set to  $(0, 0, 0)$ . Next, we define the distance vector  $d_{\text{robot}} = x_{\text{robot}} - x_{\text{object}}$ , which represents the distance from the dynamic object  $x_{\text{object}}$  to the position of the robot  $x_{\text{robot}}$ . We introduce two parameters:  $r_0$ , which defines a circular area centered at the origin point within which the objects are limited to move.  $r_1$ , which represents the threshold distance that the dynamic objects strive to maintain from the robot. Finally, we have three configurable non-negative velocity constants for the dynamic objects:  $v_0$ ,  $v_1$ , and  $v_2$ .

### A.5.1 Dynamics of targets of Chase task

$$\dot{x}_{\text{object}} = \begin{cases} v_0 * d_{\text{origin}}, & \text{if } \|d_{\text{origin}}\| > r_0 \\ -v_1 * d_{\text{robot}}, & \text{if } \|d_{\text{origin}}\| \leq r_0 \text{ and } \|d_{\text{robot}}\| \leq r_1 \\ 0, & \text{if } \|d_{\text{origin}}\| \leq r_0 \text{ and } \|d_{\text{robot}}\| > r_1 \end{cases}, \quad (8)$$

### A.5.2 Dynamics of targets of Defense task

$$\dot{x}_{\text{object}} = \begin{cases} v_0 * d_{\text{origin}}, & \text{if } \|d_{\text{origin}}\| > r_0 \\ -v_1 * d_{\text{robot}}, & \text{if } \|d_{\text{origin}}\| \leq r_0 \text{ and } \|d_{\text{robot}}\| \leq r_1 \\ v_2 * d_{\text{origin}}, & \text{if } \|d_{\text{origin}}\| \leq r_0 \text{ and } \|d_{\text{robot}}\| > r_1 \end{cases}, \quad (9)$$

### A.5.3 Dynamics of ghost and 3D ghost

$$\dot{x}_{\text{object}} = \begin{cases} v_0 * d_{\text{origin}}, & \text{if } \|d_{\text{origin}}\| > r_0 \\ v_1 * d_{\text{robot}}, & \text{if } \|d_{\text{origin}}\| \leq r_0 \text{ and } \|d_{\text{robot}}\| > r_1 \\ 0, & \text{if } \|d_{\text{origin}}\| \leq r_0 \text{ and } \|d_{\text{robot}}\| \leq r_1 \end{cases}, \quad (10)$$

## B Expeiment Details

The full GUARD codebase is available online at

<https://github.com/intelligent-control-lab/guard>

The GUARD implementation is partially inspired by Safety Gym [Ray et al., 2019] and Spinningup [Achiam, 2018] which are both under MIT license.

### B.1 Policy Settings

The hyper-parameters used in our experiments are listed in Table 19 as default.

Our experiments use separate multi-layer perception with *tanh* activations for the policy network, value network and cost network. Each network consists of two hidden layers of size (64,64). All of the networks are trained using *Adam* optimizer with learning rate of 0.01.

We apply an on-policy framework in our experiments. During each epoch the agent interact  $B$  times with the environment and then perform a policy update based on the experience collected from the current epoch. The maximum length of the trajectory is set to 1000 and the total epoch number  $N$  is set to 200 as default. In our experiments the Walker and the Ant were trained for 1000 epochs due to the high dimension.

The policy update step is based on the scheme of TRPO, which performs up to 100 steps of back-tracking with a coefficient of 0.8 for line searching.

For all experiments, we use a discount factor of  $\gamma = 0.99$ , an advantage discount factor  $\lambda = 0.95$ , and a KL-divergence step size of  $\delta_{KL} = 0.02$ .

For experiments which consider cost constraints we adopt a target cost  $\delta_c = 0.0$  to pursue a zero-violation policy.

Other unique hyper-parameters for each algorithms are hand-tuned to attain reasonable performance.

Each model is trained on a server with a 48-core Intel(R) Xeon(R) Silver 4214 CPU @ 2.2.GHz, Nvidia RTX A4000 GPU with 16GB memory, and Ubuntu 20.04.

For low-dimensional tasks, we train each model for 6e6 steps which takes around seven hours. For high-dimensional tasks, we train each model for 3e7 steps which takes around 60 hours.

### B.2 Experiment tasks

### B.3 Metrics Comparison

we report all the 72 results of our test suites by three metrics:

- The average episode return  $J_r$ .
- The average episodic sum of costs  $M_c$ .
- The average cost over the entirety  $\rho_c$ .

All of the three metrics were obtained from the final epoch after convergence. Each metric was averaged over two random seed.

Table 19: Important hyper-parameters of different algorithms in our experiments

Policy Parameter		TRPO	TRPO-Lagrangian	TRPO-SL [18' Dalal]	TRPO-USL	TRPO-IPO	TRPO-FAC	CPO	PCPO
Epochs	$N$	200	200	200	200	200	200	200	200
Steps per epoch	$B$	30000	30000	30000	30000	30000	30000	30000	30000
Maximum length of trajectory	$L$	1000	1000	1000	1000	1000	1000	1000	1000
Policy network hidden layers	$(64, 64)$	$(64, 64)$	$(64, 64)$	$(64, 64)$	$(64, 64)$	$(64, 64)$	$(64, 64)$	$(64, 64)$	$(64, 64)$
Discount factor	$\gamma$	0.99	0.99	0.99	0.99	0.99	0.99	0.99	0.99
Advantage discount factor	$\lambda$	0.97	0.97	0.97	0.97	0.97	0.97	0.97	0.97
TRPO backtracking steps		100	100	100	100	100	100	100	-
TRPO backtracking coefficient		0.8	0.8	0.8	0.8	0.8	0.8	0.8	-
Target KL	$\delta_{KL}$	0.02	0.02	0.02	0.02	0.02	0.02	0.02	0.02
Value network hidden layers	$(64, 64)$	$(64, 64)$	$(64, 64)$	$(64, 64)$	$(64, 64)$	$(64, 64)$	$(64, 64)$	$(64, 64)$	$(64, 64)$
Value network iteration		80	80	80	80	80	80	80	80
Value network optimizer		Adam	Adam	Adam	Adam	Adam	Adam	Adam	Adam
Value learning rate		0.001	0.001	0.001	0.001	0.001	0.001	0.001	0.001
Cost network hidden layers		-	$(64, 64)$	$(64, 64)$	$(64, 64)$	-	$(64, 64)$	$(64, 64)$	$(64, 64)$
Cost network iteration		-	80	80	80	-	80	80	80
Cost network optimizer		-	Adam	Adam	Adam	-	Adam	Adam	Adam
Cost learning rate		-	0.001	0.001	0.001	-	0.001	0.001	0.001
Target Cost	$\delta_c$	-	0.0	0.0	0.0	0.0	0.0	0.0	0.0
Lagrangian optimizer		-	-	-	-	-	-	-	-
Lagrangian learning rate		-	-	-	-	-	-	-	-
USL correction iteration		-	-	-	-	-	-	-	-
USL correction rate		-	-	-	-	-	-	-	-
Warmup ratio	$t$	-	-	1/3	1/3	-	0.01	-	-
IPO parameter		-	-	-	-	-	-	-	-
Cost reduction		-	-	-	-	-	-	0.0	-

Goal_Point_8Hazards	Push_Point_8Hazards
Goal_Point_8Ghosts	Push_Point_8Ghosts
Goal_Swimmer_8Hazards	Push_Swimmer_8Hazards
Goal_Swimmer_8Ghosts	Push_Swimmer_8Ghosts
Goal_Ant_8Hazards	Push_Ant_8Hazards
Goal_Ant_8Ghosts	Push_Ant_8Ghosts
Goal_Walker_8Hazards	Push_Walker_8Hazards
Goal_Walker_8Ghosts	Push_Walker_8Ghosts
Goal_Humanoid_8Hazards	Push_Humanoid_8Hazards
Goal_Humanoid_8Ghosts	Push_Humanoid_8Ghosts
Goal_Hopper_8Hazards	Push_Hopper_8Hazards
Goal_Hopper_8Ghosts	Push_Hopper_8Ghosts
Goal_Arm3_8Hazards	Push_Arm3_8Hazards
Goal_Arm3_8Ghosts	Push_Arm3_8Ghosts
Goal_Arm6_8Hazards	Push_Arm6_8Hazards
Goal_Arm6_8Ghosts	Push_Arm6_8Ghosts
Goal_Drone_8Hazards	Push_Drone_8Hazards
Goal_Drone_8Ghosts	Push_Drone_8Ghosts
<hr/>	
(a) Goal	(b) Push
<hr/>	
Chase_Point_8Hazards	Defense_Point_8Hazards
Chase_Point_8Ghosts	Defense_Point_8Ghosts
Chase_Swimmer_8Hazards	Defense_Swimmer_8Hazards
Chase_Swimmer_8Ghosts	Defense_Swimmer_8Ghosts
Chase_Ant_8Hazards	Defense_Ant_8Hazards
Chase_Ant_8Ghosts	Defense_Ant_8Ghosts
Chase_Walker_8Hazards	Defense_Walker_8Hazards
Chase_Walker_8Ghosts	Defense_Walker_8Ghosts
Chase_Humanoid_8Hazards	Defense_Humanoid_8Hazards
Chase_Humanoid_8Ghosts	Defense_Humanoid_8Ghosts
Chase_Hopper_8Hazards	Defense_Hopper_8Hazards
Chase_Hopper_8Ghosts	Defense_Hopper_8Ghosts
Chase_Arm3_8Hazards	Defense_Arm3_8Hazards
Chase_Arm3_8Ghosts	Defense_Arm3_8Ghosts
Chase_Arm6_8Hazards	Defense_Arm6_8Hazards
Chase_Arm6_8Ghosts	Defense_Arm6_8Ghosts
Chase_Drone_8Hazards	Defense_Drone_8Hazards
Chase_Drone_8Ghosts	Defense_Drone_8Ghosts
<hr/>	
(c) Chase	(d) Defense

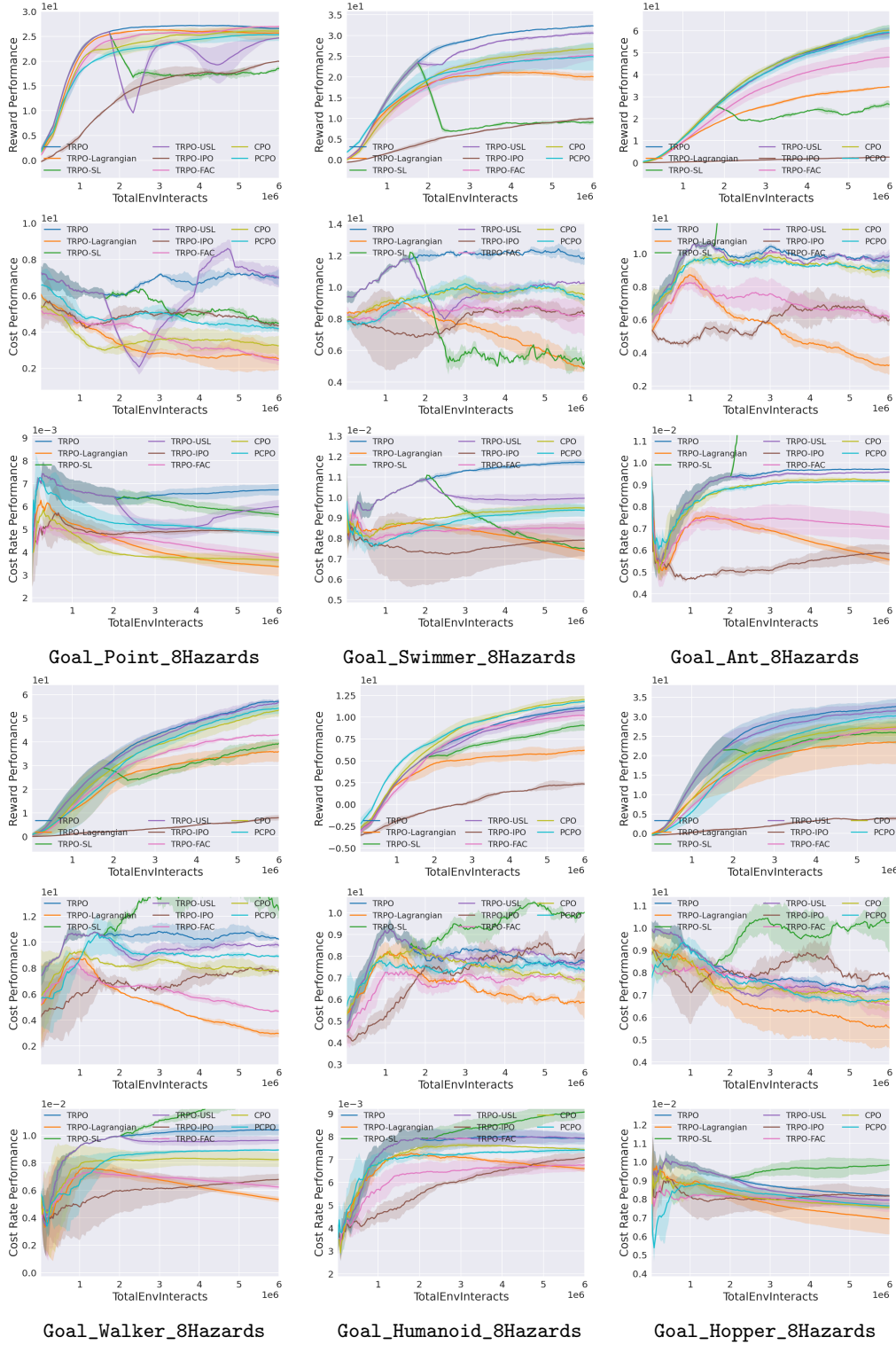
Table 20: Tasks of our environments





Table 25: Metrics of nine **Defense\_{Robot}\_8Hazards** environments obtained from the final epoch.

Defense_Point_8Hazards				Defense_Swimmer_8Hazards				Defense_Ant_8Hazards			
Algorithm	$\bar{J}_r$	$\bar{M}_c$	$\bar{\rho}_c$	Algorithm	$\bar{J}_r$	$\bar{M}_c$	$\bar{\rho}_c$	Algorithm	$\bar{J}_r$	$\bar{M}_c$	$\bar{\rho}_c$
TRPO	<b>71.7851</b>	37.5050	0.0308	TRPO	119.9896	44.5965	0.0405	TRPO	<b>65.9815</b>	46.1871	0.0214
TRPO-Lagrangian	-12.2159	1.1776	0.0026	TRPO-Lagrangian	-85.0177	<b>0.2487</b>	<b>0.0031</b>	TRPO-Lagrangian	-109.9671	1.5799	<b>0.0040</b>
TRPO-SL	-89.8828	3.1691	0.0070	TRPO-SL	-41.8928	1.3295	0.0118	TRPO-SL	-15.0035	14.7914	0.0143
TRPO-USL	-109.7828	9.9285	0.0086	TRPO-USL	<b>139.8915</b>	13.5482	0.0150	TRPO-USL	-9.1186	25.8625	0.0126
TRPO-IPO	-330.4252	<b>0.7309</b>	0.0035	TRPO-IPO	-233.1962	7.6313	0.0070	TRPO-IPO	-205.8713	6.0119	0.0044
TRPO-FAC	-269.0397	0.7334	<b>0.0015</b>	TRPO-FAC	-91.7454	0.8809	0.0032	TRPO-FAC	-204.4595	<b>1.4105</b>	0.0041
CPO	36.7643	7.1534	0.0071	CPO	34.3226	2.7346	0.0072	CPO	-22.6369	17.9356	0.0132
PCPO	19.0943	1.9388	0.0048	PCPO	91.1387	5.1068	0.0084	PCPO	-42.0119	17.1633	0.0120
Defense_Walker_8Hazards				Defense_Humanoid_8Hazards				Defense_Hopper_8Hazards			
Algorithm	$\bar{J}_r$	$\bar{M}_c$	$\bar{\rho}_c$	Algorithm	$\bar{J}_r$	$\bar{M}_c$	$\bar{\rho}_c$	Algorithm	$\bar{J}_r$	$\bar{M}_c$	$\bar{\rho}_c$
TRPO	<b>63.0381</b>	52.1661	0.0326	TRPO	-279.6928	4.3248	0.0042	TRPO	-79.4386	26.9427	0.0202
TRPO-Lagrangian	-221.9464	<b>0.8080</b>	<b>0.0032</b>	TRPO-Lagrangian	-287.5846	3.0248	0.0035	TRPO-Lagrangian	-304.2345	1.1963	<b>0.0029</b>
TRPO-SL	-28.2392	21.2179	0.0142	TRPO-SL	-325.6846	2.0650	0.0039	TRPO-SL	-207.0506	8.9198	0.0138
TRPO-USL	19.2097	23.4844	0.0182	TRPO-USL	-318.2901	3.5935	0.0043	TRPO-USL	<b>57.7316</b>	28.5037	0.0234
TRPO-IPO	-213.4079	2.7606	0.0045	TRPO-IPO	-281.2530	4.3968	0.0038	TRPO-IPO	-248.0784	6.6735	0.0046
TRPO-FAC	-183.6202	1.6905	0.0035	TRPO-FAC	-271.4645	<b>2.0044</b>	<b>0.0034</b>	TRPO-FAC	-233.1694	<b>0.7496</b>	0.0038
CPO	32.0705	14.7761	0.0151	CPO	<b>-246.6409</b>	5.8980	0.0049	CPO	-271.5419	8.3413	0.0077
PCPO	43.8441	17.0562	0.0161	PCPO	-317.0349	2.9953	0.0040	PCPO	-279.4999	7.2803	0.0077
Defense_Arm3_8Hazards				Defense_Arm6_8Hazards				Defense_Drone_8Hazards			
Algorithm	$\bar{J}_r$	$\bar{M}_c$	$\bar{\rho}_c$	Algorithm	$\bar{J}_r$	$\bar{M}_c$	$\bar{\rho}_c$	Algorithm	$\bar{J}_r$	$\bar{M}_c$	$\bar{\rho}_c$
TRPO	169.5352	22.0750	0.0301	TRPO	<b>183.9203</b>	56.5334	0.0548	TRPO	-241.5720	0.0771	0.0002
TRPO-Lagrangian	151.7291	<b>0.7971</b>	<b>0.0056</b>	TRPO-Lagrangian	169.9900	<b>1.0108</b>	<b>0.0045</b>	TRPO-Lagrangian	-245.7311	0.2276	0.0002
TRPO-SL	112.3637	1.1085	0.0160	TRPO-SL	171.8430	13.3277	0.0229	TRPO-SL	-371.7727	<b>0.0000</b>	<b>0.0001</b>
TRPO-USL	164.4992	5.3212	0.0163	TRPO-USL	183.7060	52.3346	0.0528	TRPO-USL	-336.7727	0.2161	0.0001
TRPO-IPO	94.1636	9.1085	0.0171	TRPO-IPO	127.3447	3.8719	0.0051	TRPO-IPO	-275.5550	0.2600	0.0002
TRPO-FAC	<b>180.9871</b>	1.7731	0.0064	TRPO-FAC	175.8257	2.3101	0.0109	TRPO-FAC	-215.4844	0.0691	0.0001
CPO	167.4984	16.4595	0.0162	CPO	174.7701	22.8158	0.0346	CPO	<b>-212.1858</b>	0.0236	0.0002
PCPO	160.2841	22.2282	0.0189	PCPO	174.4207	30.1276	0.0264	PCPO	-219.4308	0.3358	0.0003



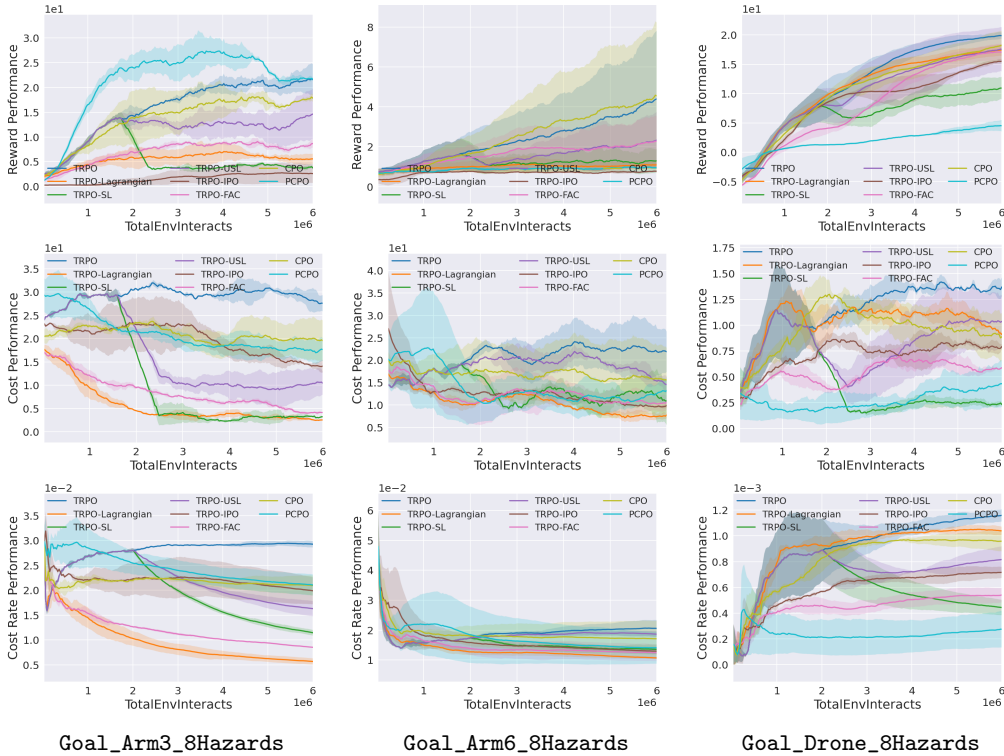
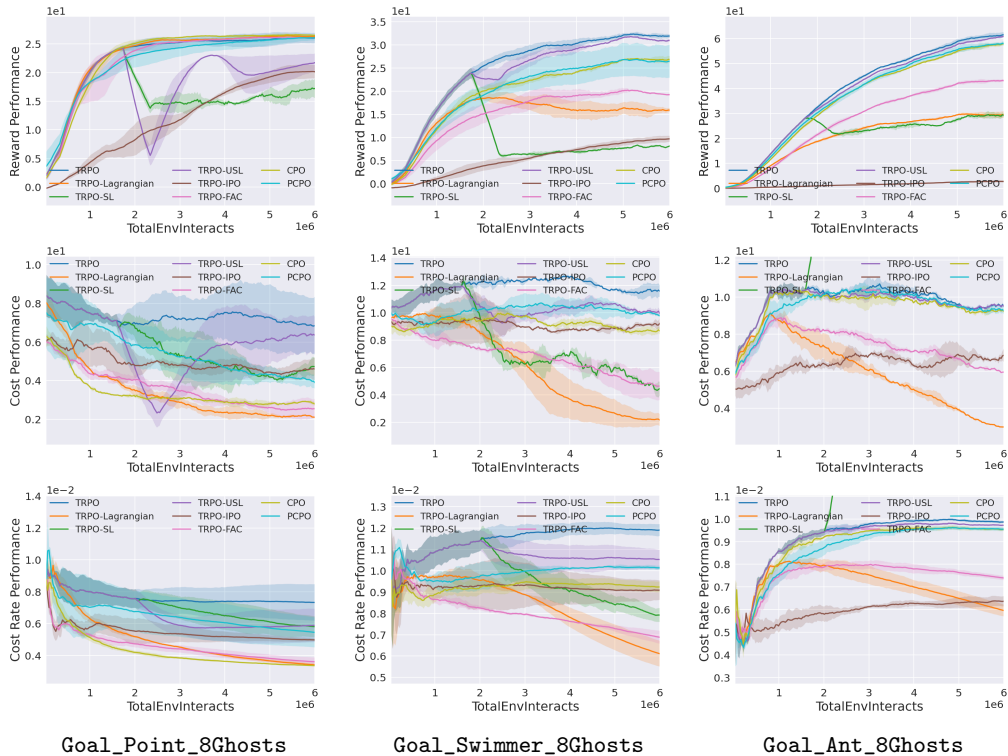


Figure 6: Goal\_{Robot}\_8Hazards



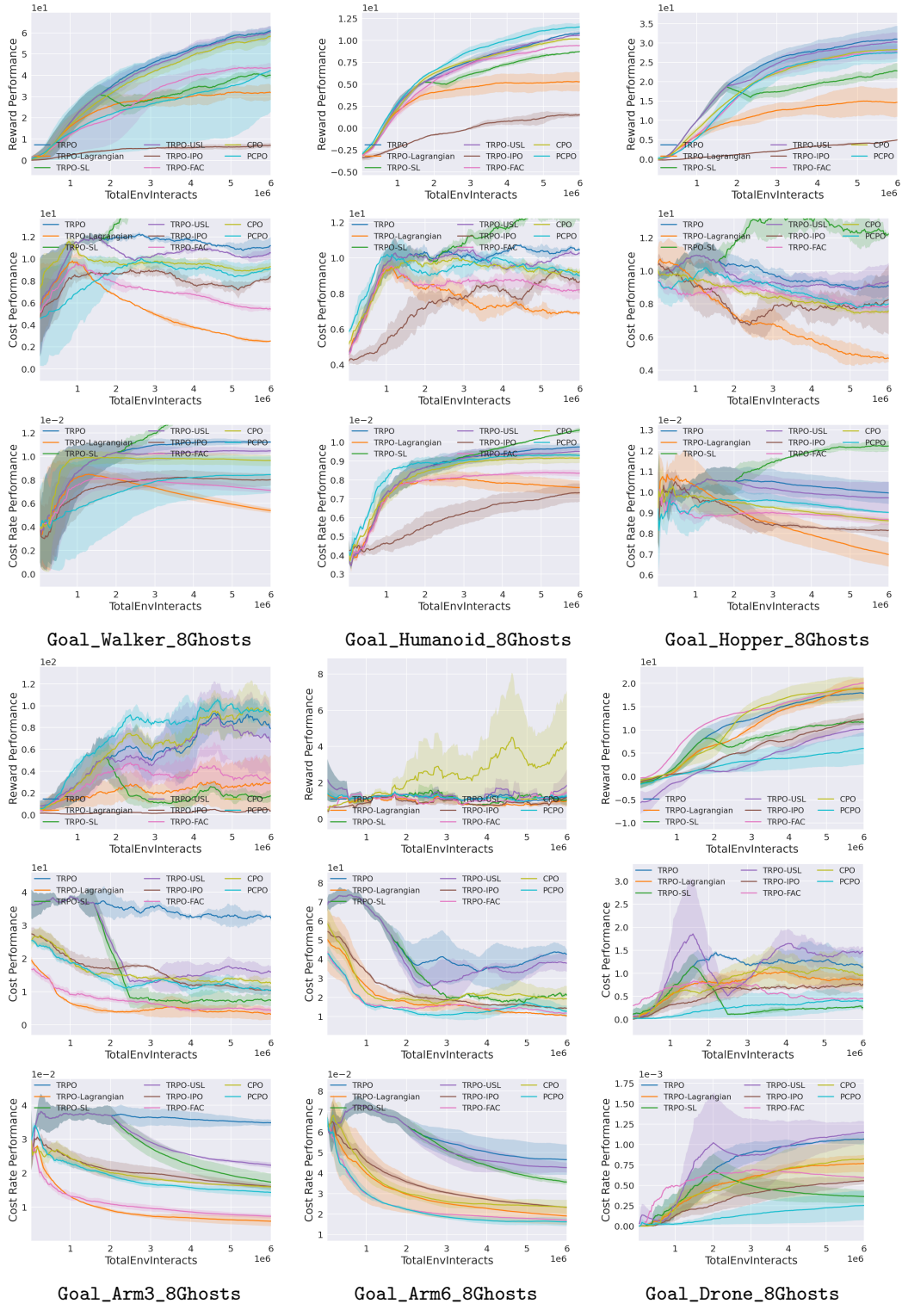
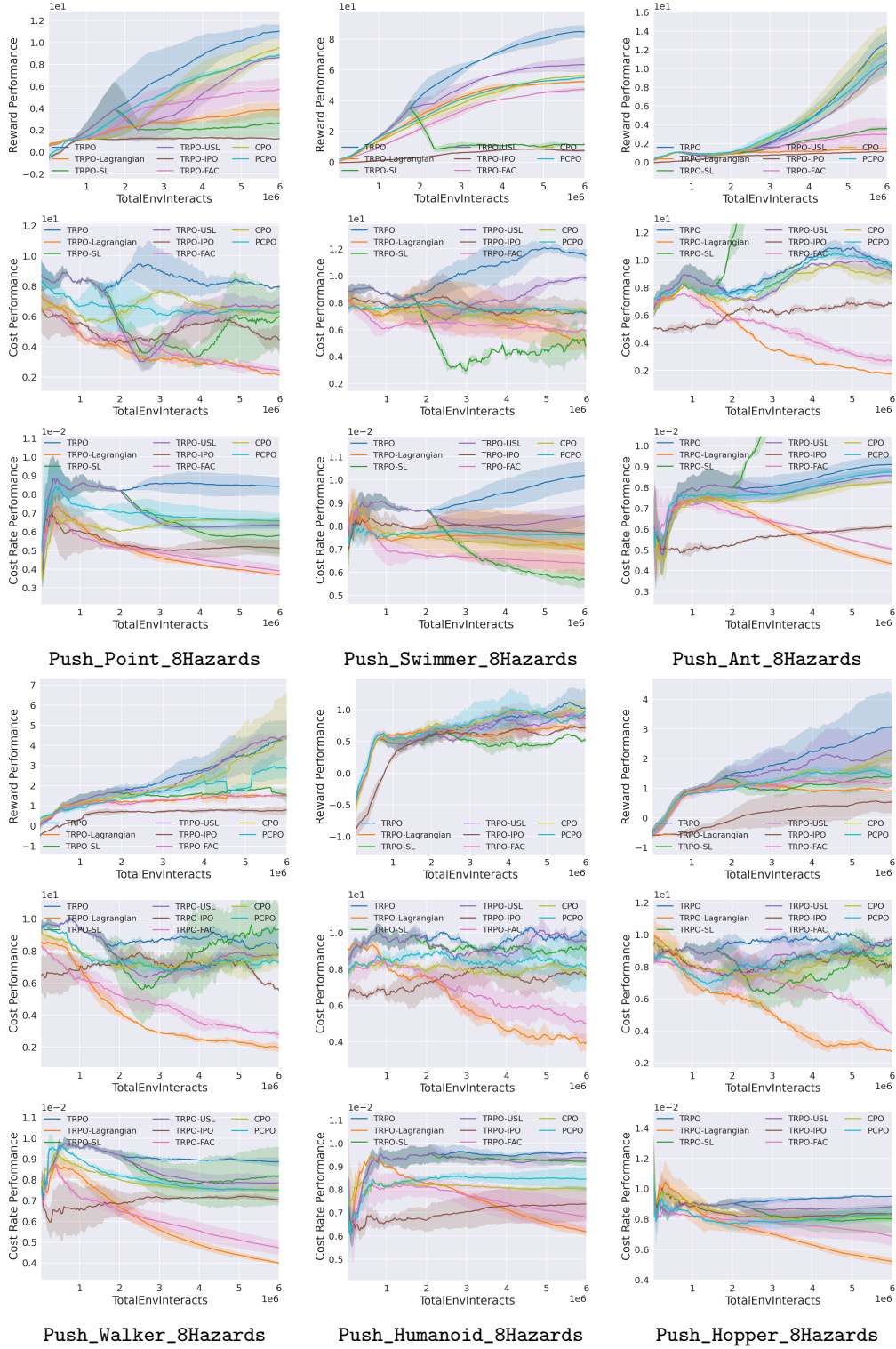


Figure 7: Goal\_{Robot}\_8Ghosts



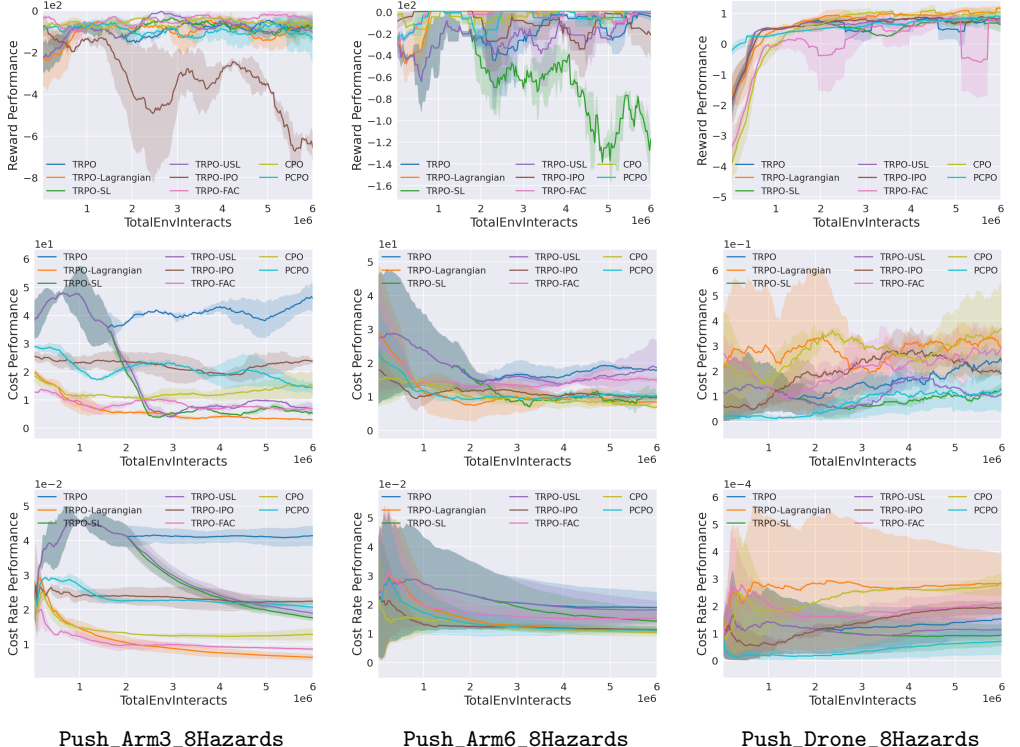
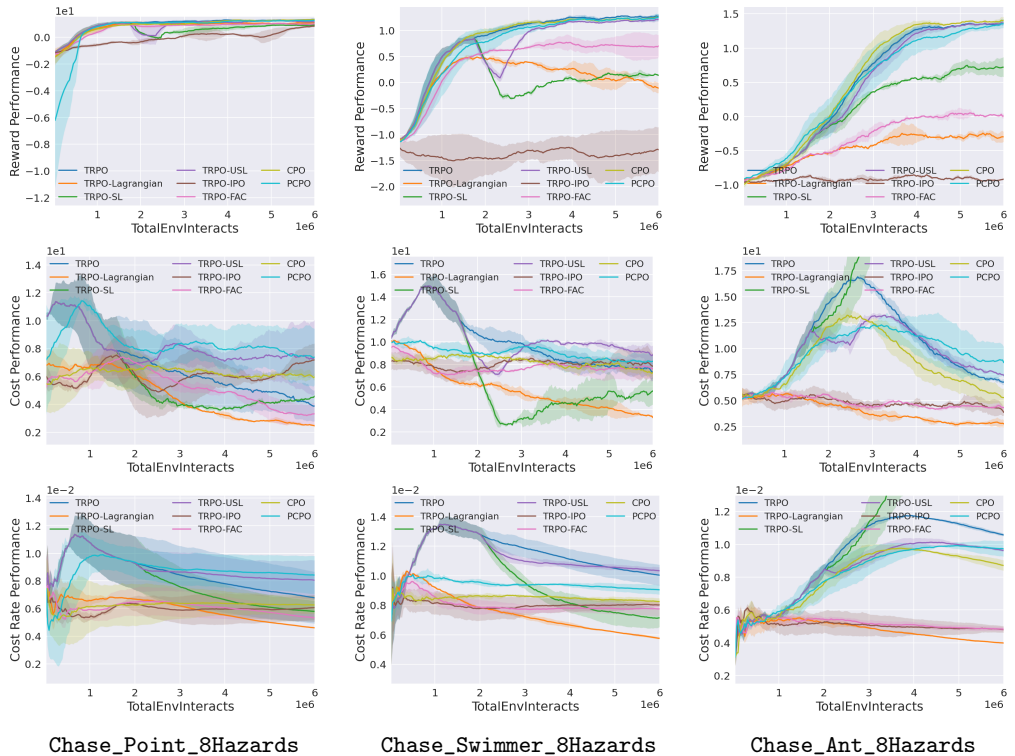


Figure 8: Push\_{{Robot}}\_8Hazards



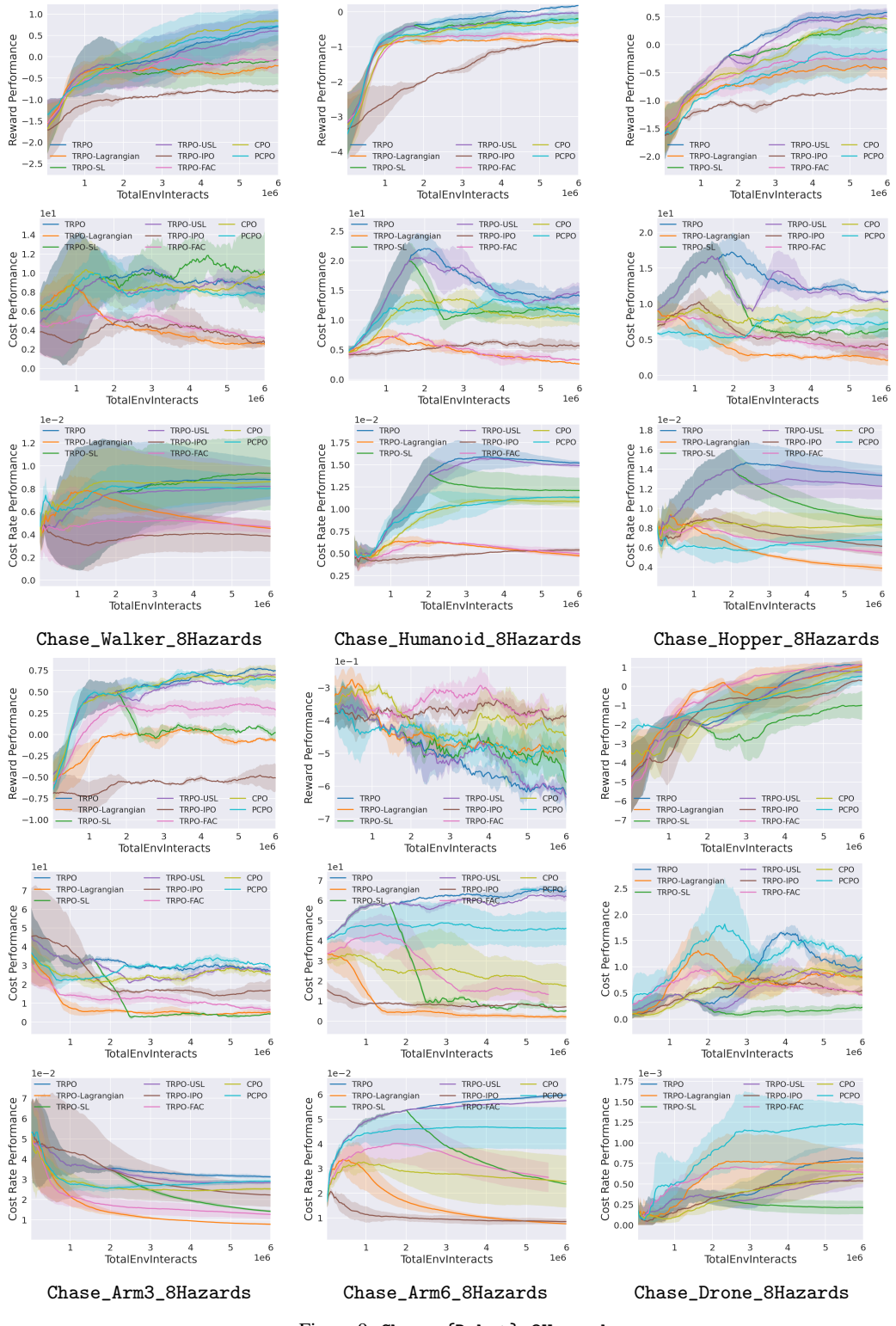
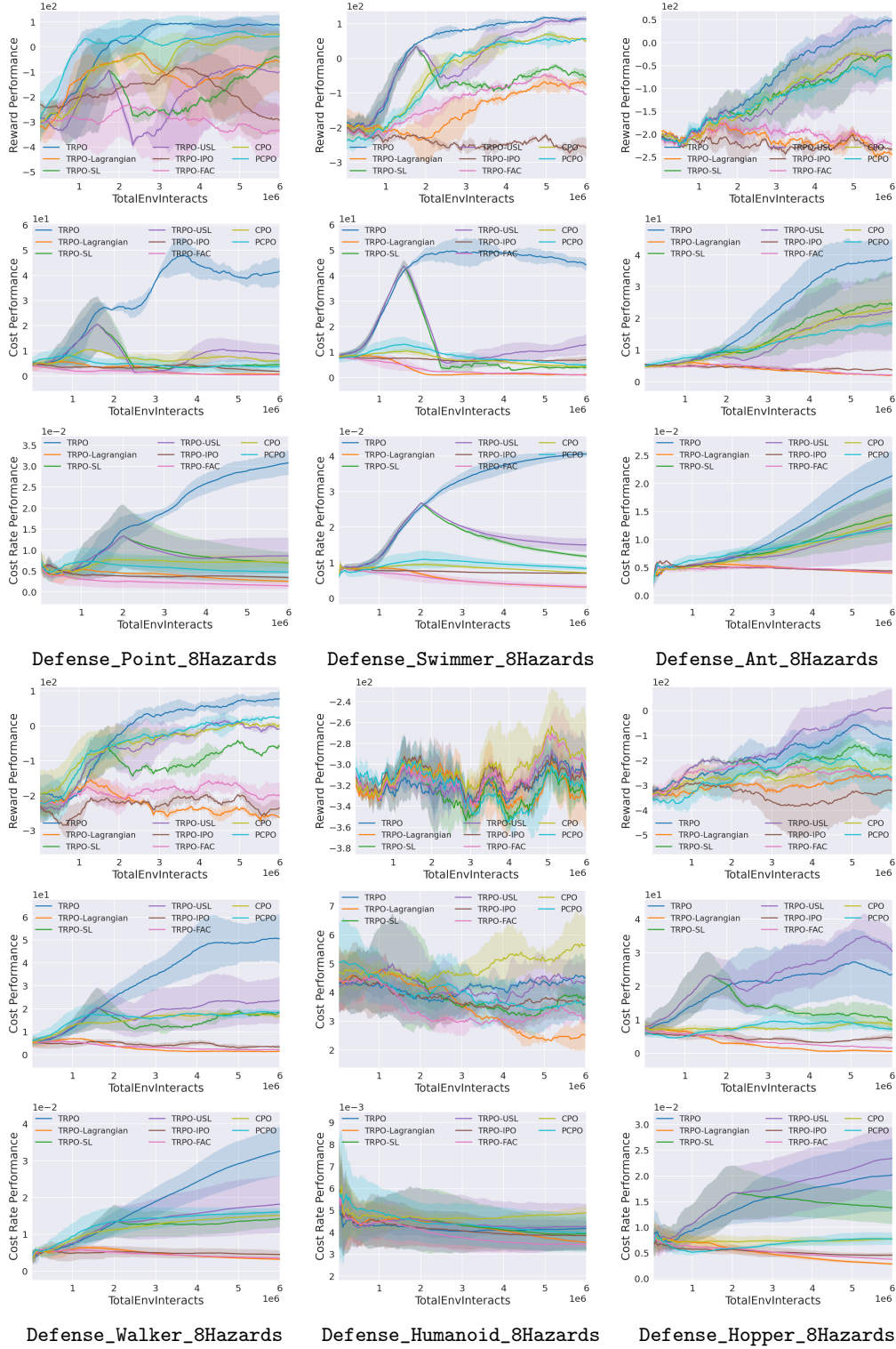


Figure 9: Chase\_{Robot}\_8Hazards



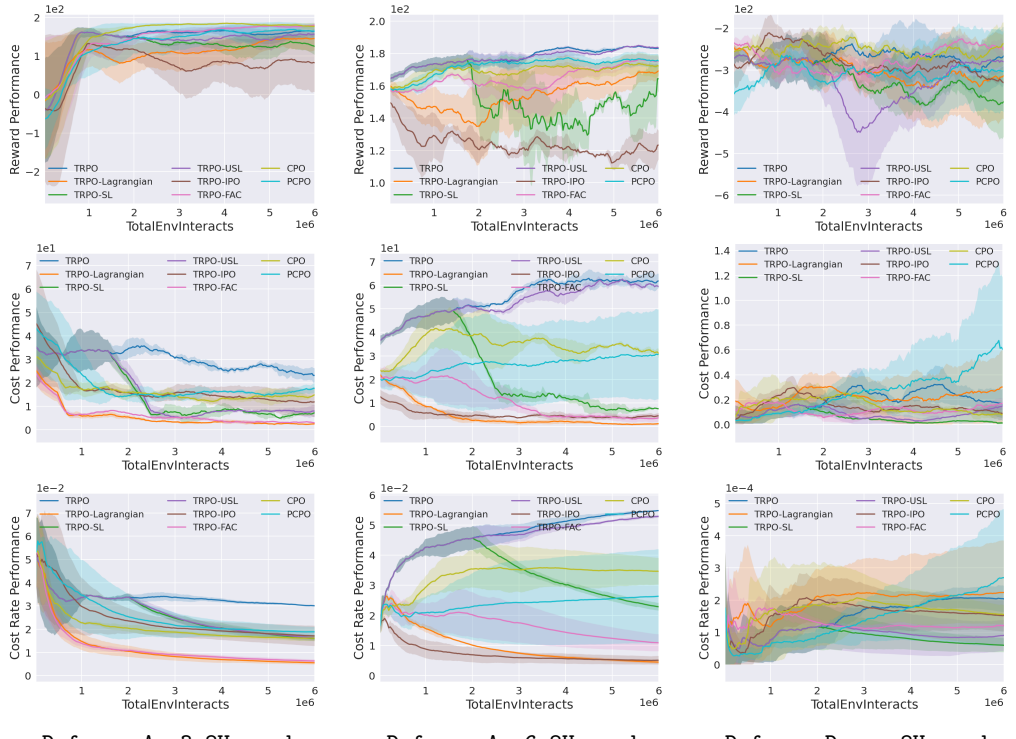


Figure 10: Defense\_{{Robot}}\_8Hazards